



UPPSALA
UNIVERSITET



Versuchsanstalt für Wasserbau,
Hydrologie und Glaziologie

Characterizing the morphology of Griesgletscher's subglacial drainage system

Marie Selenius

ABSTRACT

Characterizing the morphology of Griesgletscher's subglacial drainage system

Marie Selenius

The bedrock under Griesgletscher is formed in a bowled-shaped cavity, an overdeepening. This is known to affect the flow of ice and subglacial water by causing inefficient drainage through the overdeepening. This report aims to, from field data, investigate what further consequences overdeepenings might have for subglacial drainage mechanisms and seasonal evolution.

A field campaign was performed at Griesgletscher, Switzerland, during the summer 2017. Turbidity, discharge and electrical conductivity were monitored in a proglacial stream throughout the ablation season. 115 water samples were collected for calibration of the turbidity measurements and the relationship between the concentration of suspended sediments in the meltwater and the magnitude of discharge was investigated through simple and multiple linear regression. In addition, ten tracer experiments were conducted by injecting dye in moulins on the glacier tongue, and measuring the fluorescence of the water in the proglacial streams.

The results obtained during the field campaign suggest that the main part of the overdeepened area at Griesgletscher is drained via a lateral channel passing around the overdeepening and that subglacial water from the overdeepening is drained at times of high discharge. The driving force for drainage of subglacial water from the overdeepening is suggested to be the gradient created from rising water pressure in the ice above the overdeepening. Results further suggest that subglacial drainage at a part of the adverse slope is inefficient and remains inefficient throughout the ablation season. This differs from the seasonal evolution normally seen at non-overdeepened glaciers, in which an efficient, channelized system evolves during the course of the season.

Keywords: glacial hydrology, subglacial drainage, overdeepenings, dye-tracing, glacial sediment yield, suspended sediment transport, regression analysis

Department of Earth Science, Program of Air, Water and Landscape Science, Uppsala University. Villavägen 16, SE-75236, Uppsala, Sweden

REFERAT

Karaktärisering av Griesgletschers subglaciala dräneringssystem

Marie Selenius

Formen på berggrunden under en glaciär är avgörande för flödet av smältvatten och is. Det är vanligt att berggrunden under en glaciär utgör en skålformad fördjupning kallad överfördjupning. Det är sedan tidigare känt att flödet genom överfördjupningar är begränsat och forskning tyder på att smältvatten tenderar att välja kanaler över eller runt överfördjupningen i de fall då sådana finns tillgängliga. Många frågor kvarstår dock gällande vilken betydelse överfördjupningar har för det subglaciala dräneringssystemet och dess säsongsutveckling och antalet fältstudier som berör ämnet är få. Den här rapporten syftar till att, från fältdata, tillföra kunskap om överfördjupningars inverkan på subglacial dränering.

Under sommaren 2017 utfördes en fältstudie på Griesgletscher, en överfördjupad glaciär belägen i de Schweiziska alperna. Turbiditet, elektrisk konduktivitet och flöde mättes i en av de proglaciära smältbäckarna. 115 vattenprover samlades in för bestämning av koncentrationen suspenderade sediment och användes för att omvandla mätningar av turbiditet till koncentration av suspenderade sediment. Relationen mellan transport av suspenderade sediment och flöde kunde sedan undersökas genom enkel och multipel linjär regression. I tillägg utfördes tio försök då ett fluorescerande spårämne injicerades i en moulin på glaciärtungan och fluorescensen mättes i smältbäckarna som avrinner från Griesgletscher. Utifrån resultaten kunde Griesgletschers dräneringssystem och dess utveckling kartläggas.

De resultat som uppnåtts under fältstudien tyder på att det överfördjupade området av Griesgletscher i huvudsak dräneras via en sidokanal som passerar runt överfördjupningen samt att subglacialt vatten från överfördjupningen främst dräneras vid högt flöde. Drivkraften för dränering av subglacialt vatten från överfördjupningen föreslås vara den gradient som skapas vid hög avrinning, då vattentrycket i isen ovanför överfördjupningen stiger. Resultatet från de regressionsanalyser som utförts visade sig vara representativt enbart för en del av överfördjupade området. Tolkningar av resultaten tyder på att det subglaciala dräneringssystemet i detta område var ineffektivt att evakuera smältvatten och förblev ineffektivt under hela smältsäsongen. Detta skiljer sig från den säsongsmässiga utvecklingen som normalt kan ses på glaciärer utan överfördjupning, där ett effektivt kanaliserat dräneringssystem utvecklas under sommaren. Slutligen kunde graden av flöde fastställas som den viktigaste drivvariabeln för koncentrationen av suspenderade sediment i smältvattnet tillsammans med förändringen av flöde, tidigare koncentration av suspenderade sediment och nederbörd.

Nyckelord: glacialhydrologi, subglacial dränering, överfördjupningar, spårämnesförsök, glacial sedimentproduktion, transport av suspenderade sediment, regressionsanalys

Institutionen för Geovetenskaper, Luft- vatten- och landskapslära, Uppsala Universitet. Villavägen 16, SE-75236 Uppsala, Sverige

PREFACE

Characterizing the morphology of Griesgletscher's subglacial drainage system

Marie Selenius

This Master Thesis makes the final part of the M.Sc. in Environmental and Water Engineering at Uppsala University and the Swedish University of Agricultural Science. The Thesis corresponds to 30 ECTS Credits and was conducted during an exchange semester at ETH Zurich at the Laboratory of Hydraulics, Hydrology and Glaciology, VAW. In Zurich the thesis was made in collaboration with the Swiss Federal Research Institute, WSL. Supervisor of this thesis was Professor Daniel Farinotti, Laboratory of Hydraulics, Hydrology and Glaciology, VAW, and the Swiss Federal Research Institute, WSL. The work and field campaign performed within this thesis was also supervised by Darrel Swift from University of Sheffield, Department of Geography. Subject reviewer was Rickard Petersson, Uppsala University, Department of Earth Sciences. Working with this thesis has in many ways been an interesting, challenging and new experience for me. I am very happy to have taken part of this project and to gain knowledge about glaciers that is a new, but appealing area to me. I am also very thankful for support from the Heyning-Roelli Foundation and the Swiss-European Mobility Program, that made my exchange semester in Zurich possible.

I want to send big greetings to Daniel and Darrel who always gave great support and inputs and thank you also for your positive attitude and big motivation.

I want to thank the group at WSL and VAW for a very good time. A special thanks to everyone who came to help out during the field work, carrying heavy equipment or in other ways giving a helping hand. It was always a pleasure to share this time with you. At last I want to thank Nadine Feiger for a good collaboration, for evaluation of salt dilution experiments and modeling of discharge. And for sharing the digital elevation model for the bedrock of Griesgletscher.

Copyright © Marie Selenius and the Department of Earth Sciences, Program of Air, Water and Landscape Science, Uppsala University.

UPTEC W 17 039, ISSN 1401–5765

Published digitally at the Department of Earth Sciences, Uppsala University, Uppsala 2018.

POPULÄRVETENSKAPLIG SAMMANFATTNING

Karaktärisering av Griesgletschers subglaciala dräneringssystem

Marie Selenius

Vi lever i en tid då den globala uppvärmningen blir allt mer påtaglig och jordens glaciärer smälter i ökande takt. Detta gör att kunskap om avrinning från glaciärer samt transport av sediment idag är viktigare än någonsin, då det på olika sätt påverkar vår natur. Dagens samhälle är beroende av energi och artificiella dammar nedströms från glaciärer utgör en viktig energikälla i många delar av världen. Genom att kunna förutsäga hur stor avrinning och sedimenttransport som väntas kan energiutvinningen effektiviseras.

En avgörande faktor för flödet av is, vatten och sediment är formen på berggrunden under en glaciär. Ett vanligt förekommande fenomen är att berggrunden under en glaciär utgör en skålformad fördjupning. Denna form kallas för överfördjupning och om glaciären smälter kommer en sjö att bildas i fördjupningen. Det är idag känt att överfördjupningar påverkar flödet av vatten och is, men exakt vilka konsekvenser detta har är fortfarande okänt och antalet fältstudier som behandlar ämnet är få. Den här rapporten syftar till att utreda hur transporten av smältvatten påverkas av en överfördjupning genom att utföra en fältstudie på Griesgletscher, en överfördjupad glaciär belägen i de Schweiziska alperna.

Transport av smältvatten genom en glaciär kan ske via smältkanaler på glaciärens yta, supraglacialt, eller genom kanaler genom isen, englacialt, eller följa berggrunden under glaciären, subglacialt. I den här rapporten studerades främst det subglaciala dräneringssystemet som kan delas in i två delar. Den första delen består av kanaler längs botten av glaciären som effektivt kan transportera vatten. Den andra delen täcker en stor yta av berggrunden under glaciären och vatten sipprar fram utspjutt som ett täcke under glaciären eller rinner genom håligheter och kanaler som skapats mellan berggrunden och isen på grund av erosion eller rörelse av glaciären. Den här delen av det subglaciala dräneringssystemet är mindre effektivt för transport av vatten. Smältvatten som mynnar ut från glaciärer bär med sig suspenderade sediment. Detta är produkter från erosion och vittring av berggrunden som har finfördelats tillräckligt mycket för att transporteras av smältvattnet. Vattnets hastighet är avgörande för hur mycket suspenderat sediment det kan bära med sig. Vatten som färdas snabbt har mer energi för att plocka upp och omsätta sediment än vatten som färdas med låg hastighet. Genom att mäta sedimenttransporten i smältvattnet från en glaciär och hur detta förändras med förändrat flöde kan således det subglaciala dräneringssystemet studeras och antagande göras om vilken del av det subglaciala dräneringssystemet som dominerar. På vintern, när avsmältningen avtar, fryser en stor del av de kanaler som dränerat vatten under sommarmånaderna. På våren när avsmältningen börjar tillta igen är det subglaciala dräneringssystemet därför ineffektivt att transportera smältvatten och domineras av ett distribuerat, långsamt dräneringssystem. I takt med att avsmältningen tilltar utvecklas normalt ett nätverk av kanaler som effektivt kan transportera smältvatten bort från glaciären. Idag är det dock okänt om denna utveckling infinner sig även på överfördjupade glaciärer.

En fältstudie utfördes på Griesgletscher under sommaren 2017. Smältvattnet från

Griesgletscher lämnar huvudsakligen glaciären via tre smältvattenbäckar. En mätstation installerades i en av bäckarna i början av juli och mätningar fortgick fram till början av september. Turbiditet (grumlighet), flöde samt elektrisk konduktivitet (ledningsförmåga) mättes kontinuerligt under perioden. 115 vattenprover samlades också in och koncentrationen av suspenderade sediment fastställdes. Provresultaten kunde sedan användas för att omvandla mätningarna av turbiditet till koncentration av suspenderade sediment.

Elektrisk konduktivitet är ett mått på koncentrationen av joner i smältvattnet. För vatten som uppehållit sig länge i dräneringssystemet och i kontakt med berggrunden, kan en hög koncentration av joner förväntas. Den elektriska konduktiviteten kan på så sätt ge en indikation av hur länge vattnet färdats genom dräneringssystemet.

Utöver mätningarna i smältvattenbäcken utfördes tio spårämnesförsök. Ett fluorescerande självlysande spårämne injicerades då i en moulin, ett naturligt hål ovanpå glaciären med anslutning till dräneringssystemet. Fluorescensen mättes sedan i bäckarna nedströms från glaciären och gav en bild över dräneringssystemets uppbyggnad samt hur lång tid det tog för smältvatten att färdas genom dräneringssystemet. Utav de tre smältvattenbäckar som lämnar Griesgletscher, mynnar den största ut på den högra sidan av glaciären. Spårämnesförsök tydde på att den största delen av smältvattnet från det överfördjupade området dränerades via denna bäck. Vidare kunde en stor skillnad i grumlighet observeras i just denna bäck. På morgonen var vattnet klart men mitt på dagen, i takt med att avrinningen från glaciären ökade, blev vattnet allt mer grumligt. Det klara vattnet tros ha varit smältvatten som dränerats via en kanal som passerar längs den högra sidan av överfördjupningen. Det grumliga vattnet, å andra sidan, tros härstamma från överfördjupningen, där tillgången till sediment är stor. Resultaten tydde vidare på att subglacialt vatten från överfördjupningen främst dränerades då avrinningen från glaciären var stor, det vill säga mitt på dagen då temperatur och solstrålning orsakade större smältning av snö och is. En förklaring skulle kunna vara att då flödet tilltog var sidokanalen inte längre tillräcklig för att evakuera tillförseln av smältvatten. Alltså tillfördes mer vatten till det överfördjupade området än vad som kunde föras bort, vilket resulterade i att vattennivån i det överfördjupade området, som normalt är i nivå med överfördjupningens kant, steg. Detta skapade i sin tur ett ökat vattentryck som tvingade subglacialt vatten ut från överfördjupningen.

Studier av sambandet mellan koncentrationen av suspenderat sediment samt mängden smältvatten tyder på att effektiviteten att evakuera suspenderade sediment var låg och förblev låg under hela sommaren. Samtidigt kunde ingen förändring i tillgången till suspenderade sediment ses. Detta tyder på att det subglaciala dräneringssystemet domineras av ett ineffektivt, distribuerat flöde. Resultatet baseras dock på mätningar gjorda i en av de tre smältbäckarna, vars avrinningsområde ej tros ha innefattat det huvudsakliga överfördjupade området. För att kunna fastställa karaktären för det subglaciala dräneringssystemet i hela det överfördjupade området av Griesgletscher krävs därför vidare studier av sedimenttransport och flöde i de tre utmynnande smältbäckarna.

GLOSSARY

Ablation season : Melt season

Englacial : Within the ice of the glacier

Moulin : Natural hole in the ice where meltwater can enter and connect to the drainage system

Orographic sequence : Streams ordered from the source to the mouth

Overdeepening : A bowl-shaped cavity in the bedrock

Proglacial : Beyond the glacier

Riegel : A ridge perpendicular to the direction of flow of ice and water

Subglacial : At the bottom of the glacial

Supraglacial : At the surface of the glacier

ABBREVIATIONS

EC Electrical conductivity

SSC Suspended sediment concentration

TB Turbidity

Q Discharge

TABLE OF CONTENT

| | | |
|----------|---|-----------|
| 1 | INTRODUCTION | 1 |
| 1.1 | AIM | 1 |
| 2 | BACKGROUND | 2 |
| 2.1 | SUBGLACIAL HYDROLOGY | 2 |
| 2.2 | TRANSPORT OF SUSPENDED SEDIMENTS | 3 |
| 2.3 | OVERDEEPENINGS | 4 |
| 2.4 | HYPOTHESIS | 7 |
| 3 | FIELD CAMPAIGN | 7 |
| 3.1 | FIELD SITE | 7 |
| 3.2 | GAUGING STATION | 8 |
| 3.2.1 | Water samples | 11 |
| 3.2.2 | Salt dilution experiments | 11 |
| 3.2.3 | Maintenance | 11 |
| 3.3 | TRACER EXPERIMENTS | 12 |
| 3.4 | FIELDWORK TIME SCHEME | 13 |
| 4 | DATA PROCESSING | 14 |
| 4.1 | PREPARATION OF DATA SET | 14 |
| 4.2 | CALIBRATION OF A TURBIDITY - SUSPENDED SEDIMENT CONCENTRATION RELATION | 14 |
| 4.3 | CALIBRATION OF A STAGE - DISCHARGE RELATION | 15 |
| 5 | RESULTS AND OBSERVATIONS | 17 |
| 5.1 | RESULTS FROM THE GAUGING STATION | 17 |
| 5.2 | FIELD OBSERVATIONS | 18 |
| 5.3 | RESULTS FROM TRACER EXPERIMENTS | 19 |
| 5.4 | SALT DILUTION EXPERIMENTS | 21 |
| 6 | SUSPENDED SEDIMENT CONCENTRATION AND DISCHARGE | 23 |

| | | |
|-----------|--|-----------|
| 6.1 | LINEAR REGRESSION | 23 |
| 6.1.1 | Theory | 23 |
| 6.1.2 | Transformation of the data | 24 |
| 6.1.3 | Approach | 24 |
| 6.1.4 | Moving window regression | 25 |
| 6.1.5 | Subperiods | 27 |
| 6.1.6 | Results | 28 |
| 6.2 | MULTIPLE LINEAR REGRESSION | 31 |
| 6.2.1 | Theory | 31 |
| 6.2.2 | Approach | 32 |
| 6.2.3 | Explanatory variables | 32 |
| 6.2.4 | Results | 33 |
| 6.3 | AUTOCORRELATION | 34 |
| 6.3.1 | Results | 35 |
| 7 | RESPONSE TO CLIMATIC VARIABLES | 37 |
| 7.1 | RESULTS | 37 |
| 8 | DISCUSSION | 38 |
| 8.1 | GRIESGLETSCHER'S SUBGLACIAL DRAINAGE SYSTEM | 38 |
| 8.2 | SEASONAL EVOLUTION OF THE SUBGLACIAL DRAINAGE SYSTEM | 41 |
| 8.3 | COMPARISON TO NON-OVERDEEPEENED GLACIERS | 43 |
| 8.4 | PRACTICAL CONSIDERATIONS AND ENCOUNTERED PROBLEMS | 44 |
| 9 | CONCLUSION | 47 |
| 10 | REFERENCES | 48 |
| | Appendices | 51 |
| | APPENDIX A Calibration of turbidity measurements | 51 |
| | APPENDIX B Calculation of discharge | 53 |

| | | |
|------------|--|----|
| APPENDIX C | Plot variables and weather data | 55 |
| APPENDIX D | Linear regression | 56 |
| APPENDIX E | Moving window regression | 60 |
| APPENDIX F | Intercepts from moving window regression | 61 |
| APPENDIX G | Multiple linear regression | 62 |

1 INTRODUCTION

The shape of the bedrock underneath a glacier affects the flow of ice and subglacial water. Overdeepenings are bowl-shaped cavities in the bedrock and the presence of an overdeepening under a glacier forces the subglacial water to travel up along an adverse slope to exit the overdeepening (Hooke, 1991). This is known to affect the morphology of the subglacial drainage system, as the adverse slope causes efficient subglacial channels to close (Alley et al., 1998) and water to distribute over the bed (Creys and Clarke, 2010). But, the impact this will have on subglacial drainage mechanisms and seasonal evolution is still not fully understood. In a warming climate, where the world's glaciers are melting, knowledge of glacial hydrology and sediment evacuation processes that could be used for future predictions is more important than ever. Dams built downstream of glaciers are common and serve as energy sources. Prediction of runoff and sediment evacuation can be useful to make energy production more efficient.

The inaccessibility of the subglacial drainage system complicates the investigation of subglacial mechanisms. The drainage system has in previous studies been investigated by monitoring of discharge and suspended sediments in proglacial streams (Willis et al., 1996; Hodgkins, 1999; Hodson and Ferguson, 1999; Swift et al., 2005) as the relationship between glacial discharge and fluvial transport of suspended sediments can reveal important information about the morphology of the subglacial drainage system. However, the amount of field studies performed at overdeepened glaciers is very limited. Overdeepenings are a common phenomenon and knowledge of how they affect drainage and sediment evacuation could be implemented in ice erosion models and in that way contribute to quantify their significance.

This thesis aims to add new knowledge about drainage system morphology for glaciers with overdeepenings by performing an extensive field study at Griesgletscher. Water pressure, turbidity (TB) and electrical conductivity (EC) were monitored in one of the proglacial streams during the melt season 2017 in order to evaluate the relationship between suspended sediment concentration (SSC) and discharge (Q) as well as timing and seasonal evolution. Tracer experiments provided additional information about the morphology of the drainage system.

1.1 AIM

This thesis aims to partially fill the knowledge gap of how overdeepenings affect the subglacial drainage mechanisms and seasonal evolution by conducting a case study at an overdeepened glacier, Griesgletscher. More specifically the goal was to answer the following questions:

- What are the morphological characteristics of Griesgletscher's subglacial drainage system?
- Does the morphology of Griesgletscher's subglacial drainage system evolve throughout the ablation season?
- Does the morphology of Griesgletscher's subglacial drainage system differ from the characteristics of a non-overdeepened glacier?

2 BACKGROUND

Here follows a description of subglacial hydrology, transport of suspended sediments and overdeepenings focused on alpine glaciers.

2.1 SUBGLACIAL HYDROLOGY

Glacial discharge originates from melt of ice and snow, rainfall and groundwater as well as from water stored in pockets within the glacier. The discharge follows one of the main routes, either at the bottom of the glacier along the bed, subglacially, through the glacier ice sheet, englacially or at the glacier surface, supraglacially. How big the discharge is depends on how big the input of water is, which in turn depends on meteorological factors such as global radiation, temperature and precipitation. But, the size of the discharge emerging from a glacier also depends on the structure of the drainage system and the hydraulic circumstances prevailing on the glacier (Röthlisberger and Lang, 1987).

The subglacial drainage system has typically been described to consist of two parts, where one part is described as channelized and the other part as distributed. As the distributed system at some parts also form channels Nye and Frank (1973), Raymond et al. (1995) and Fountain and Walder (1998) suggested to instead refer to these two parts as the fast subglacial drainage system and the slow subglacial drainage system. This naming will be used in this thesis. The fast part of the subglacial drainage system can be described as a channelized, convergent system that effectively evacuates water through channels called R-channels (Röthlisberger channels) (Röthlisberger, 1972). The discharge response is big also to a small change of the fast drainage systems volume (Fountain and Walder, 1998). The morphology of the slow part of the subglacial drainage system can take different forms and consists mostly of both discharge spreading out and moving as a sheet along the bed, but also as water flowing through gaps, or cavities, that are formed between the bottom of the glacier and the bed as the glacier moves (Fountain and Walder, 1998) or channels carved into the bedrock. These channels are called N-channels (Nye channels) (Paterson, 1981). In contrary to the fast system, the discharge response also to large changes in the slow drainage systems volume is small. Furthermore, the area of the bed covered by a slow subglacial drainage system is big compared to a fast subglacial drainage system (Fountain and Walder, 1998).

Diurnal, seasonal and annual discharge cycles have been observed at alpine glaciers, and are controlled mainly by the climatic factors global radiation and temperature (Röthlisberger and Lang, 1987). Field data from Aletschgletscher, Switzerland, confirmed the connection between discharge and global radiation and that a peak of radiation is followed by a peak in discharge (Röthlisberger and Lang, 1987). A typical hydrograph describing subglacial discharge show two patterns, where one is describing a quickflow with a diurnal peak, and at the other one show a more even, delayed curve (Tangborn et al., 1975). Moreover, studies have shown that the relative volume between the quick and the delayed discharge changes seasonally. As explained above, this is an effect of changes in both input of discharge and the structure of the drainage system (Röthlisberger and Lang, 1987; Nienow et al., 1998).

Seasonal changes in drainage system morphology have been observed in various

studies. To mention a few, Hock and Hooke (1993) described seasonal and diurnal variation in discharge and drainage system morphology based on tracer experiments performed at Storglaciären, Sweden. Moreover, Swift et al. (2005) confirmed a change in drainage system morphology and discharge both diurnally and throughout the ablation season by monitoring evacuation of basal suspended sediment at Haut Glacier d’Arolla.

In the beginning of the ablation season, the melt increases, but the drainage system is often limited and not yet efficient enough to evacuate the increasing amount of discharge. This creates a high water pressure within the glacier (Iken et al., 1983) as water that can not be evacuated will be stored within the glacier (Tangborn et al., 1975). Water flowing through a glacier transports heat that melts the ice around the flowing water so that conduits open and channels expand. However, when the pressure of the water is smaller than that of the ice, the conduits will again close (Röthlisberger, 1972) (Shreve, 1972). As the melt season proceeds, the drainage system keeps evolving and the development of the channels accelerates, as long as there is enough melt water and the pressure within the ice remains high. When the drainage system is well developed and can transfer melt water in a more efficient way, the water pressure will again decrease and, with it, also the development of the drainage system (Röthlisberger and Lang, 1987). When the ablation season comes to an end, melt will decrease and the drainage system that has been developed during the summer start to close so that the capacity of the system to evacuate water again decreases (Röthlisberger and Lang, 1987). Fountain and Walder (1998) as well as Raymond (1987) hypothesizes that cavities are the part of the subglacial drainage system that are most likely to survive the winter season without getting closed and that they therefore are likely to form the largest part of the subglacial drainage system when the ablation season starts. However, they also state that connections between cavities are likely to be closed by sediments or from glacial movement during the winter.

Occasionally, the diurnal cycle of discharge is interrupted by a sudden flood induced from exceptionally high melt (Gurnell, 1982), heavy rainfall (Bezinge, 1987), release of water that has been stored within the glacier (Beecroft, 1983) or a combination of these (Willis et al., 1996). Many times, these events occur in spring and are often referred to as spring flood events. Big flushes of sediments have been seen in conjunction with these events. For example at Bench Glacier, Alaska, where a flood caused by outburst of water that had been stored in the glacier because of inefficient drainage was witnessed (Anderson et al., 1999).

2.2 TRANSPORT OF SUSPENDED SEDIMENTS

Sediments in glacial areas are products from glacial and fluvial erosion, as well as from weathering (Souchez and Lorrain, 1987) and are mainly transported through the glacier by melt water (Alley et al., 1997) but also by glacial and mass movement processes (Lawson, 1995).

Suspended sediments are sediments light enough to be transported within runoff and that can be kept from sedimentation by the waters turbulence and ongoing mixing. For heavier sediments, the energy of the stream is not enough to carry the particles within it, but they are rather transported along the bed by sliding, rolling

or bouncing (Gurnell, 1987).

Willis et al. (1996) as well as Fountain (1992) stated that the transport of suspended sediments at temperate glaciers is controlled both by discharge and the morphology of the subglacial drainage system. Willis et al. (1996) concluded that changes in suspended sediment concentration can be coupled to diurnal and seasonal alterations in discharge and sediment supply as well as former evacuation of suspended sediments. Furthermore, Willis et al. (1996) confirmed that when the subglacial drainage system shifted, from being dominantly distributed to being channelized, lower concentrations of suspended sediments could be expected in the runoff. Whilst, in the beginning of the season, when the subglacial drainage system is mainly distributed, high concentrations were to be expected. However, this might be thwarted by the inefficiency of the drainage system at this time of the season.

Alley et al. (1997) described how glacial streams with a well-developed channelized drainage system can be expected to efficiently evacuate sediments during high discharge and that at this point the SSC will be limited by the sediment supply rather than by the drainage systems capacity to transport this material. This was confirmed by Swift et al. (2005). In the same study, Swift et al. (2005) stated that in the beginning of the melt season, when the drainage system was dominated by the slow subglacial drainage, the evacuation of sediments showed a slow response to increases in discharge, despite a big supply of suspended sediments. The concentration of suspended sediments in proglacial streams may decrease because of exhaustion (Gurnell, 1987). This is likely to happen at the end of the ablation season, at this state the drainage system can be expected to have shifted from being mainly slow to being fast, resulting in diminished production of new sediments (Willis, 1995). Another reason can be that most of the sediment supply has been evacuated earlier during the ablation season (e.g. Ostrem, 1975). Similar effect can be observed on diurnal or short term basis (Gurnell, 1987). Many researchers have monitored suspended sediment concentrations in proglacial streams and have created suspended sediment rating curves. In a study, similar to this one, Swift et al. (2005) examined the evolution of the drainage system of Haut Glacier d’Arolla in Switzerland during the ablation season 1998. The study showed that when the morphology of the subglacial drainage system changed, the capacity to transport suspended sediments by the melt water changed as well. The drainage systems efficiency to evacuate suspended sediments was low in the beginning of the ablation season, but at one point, in the middle of July, the efficiency increased. This was thought to be when a more efficient drainage system had developed. Haut Glacier d’Arolla is a non-overdeepened glacier and the results obtained in the study by Swift et al. (2005) agrees with previous knowledge of drainage at non-overdeepened glaciers. In this study, the relationship between SSC and Q will be examined with similar methods as was used at Haut Glacier d’Arolla and results will be compared.

2.3 OVERDEEPENINGS

An overdeepening is a bowl-shaped depression in the bedrock under the glacier, or where there used to be a glacier, created from glacial erosion (Hooke, 1991; Cook and Swift, 2012). The presence of an overdeepening means that ice, water and erosional products have to travel up along an adverse slope when leaving the overdeepening

(Figure 1). Overdeepenings are common glacial features, but the exact impact on glacial hydraulics and sediment entrainment is still not fully understood (Cook and Swift, 2012). Even so, studies agree that the presence of an overdeepening does have a big impact on the morphology of a glaciers drainage systems, seasonal and diurnal changes as well as sediment entrainment. Subglacial drainage at glaciers with overdeepenings has earlier been examined for example by measuring magnitude and fluctuations of basal water pressure (Jansson, 1995) or by tracer experiments (Hooke and Pohjola, 1994). Tracer experiments at Storglaciären showed that the biggest part of the discharge drained through englacial or lateral channels rather than passing through the overdeepening, as this was more efficient (Figure 1).

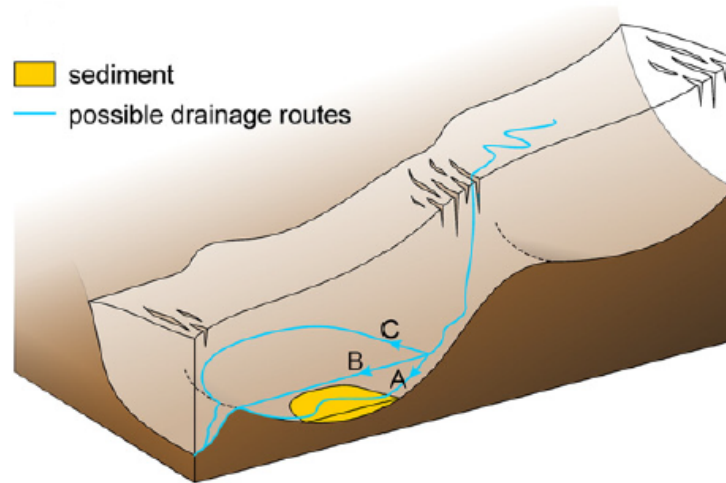


Figure 1: Possible drainage routs through an overdeepened area. Flow paths represents A) subglacial flow along the bed, B) englacial flow passing over the overdeepening and C) lateral paths around the overdeepening. Discharge following route A has to traverse the adverse slope in order to exit the overdeepening. (From Cook and Swift, 2012)

A phenomenon that has been discussed in connection with overdeepenings is supercooling. Supercooled water is found in a liquid state even though it has a temperature below its freezing point (Röthlisberger and Lang, 1987). As water rises along the adverse slope in order to leave an overdeepening, the local pressure will decrease. If the rise is fast, the water does not have time to adjust to the local pressure melting point and will therefore freeze (Röthlisberger, 1968) and in that way close channels (Hooke and Pohjola, 1994). When subglacial channels close, water will instead distribute over bed. The extent to which this occurs depends on the ratio between the gradient of the ice surface and the adverse slope (Röthlisberger and Lang, 1987).

Inefficient drainage causes basal water pressure to rise. This can be observed at non-overdeepened glaciers in the beginning of the season, when the drainage capacity is not sufficient to evacuate the increasing runoff. Later in the season, when more efficient drainage routes are established, the basal pressure decreases again. The inefficient drainage through an overdeepening, caused by the presence of the adverse slope, generates a persistent high basal water pressure within the overdeepening. Furthermore, studies made at Storglaciären, Sweden, have shown evidence

of high basal water pressure in overdeepened areas that remained high through the whole ablation season, despite variations in discharge. At areas downglacier from the overdeepening, bigger fluctuations of water pressure was observed (Jansson, 1995). This suggests the creation of an efficient, channelized drainage system after the overdeepening, whilst the subglacial drainage system in the overdeepened area remained inefficient (Jansson, 1995). Cook and Swift (2012) hypothesized that, as an effect of the inefficient drainage through overdeepenings, also the drainage system in the area above the overdeepening will be inefficient, if the discharge can not drain through englacial or lateral channels. Cook and Swift (2012) discussed how seasonal changes of basal water pressure within overdeepened areas could differ from a non overdeepened area and how this would affect the drainage morphology (Figure 2). High basal water pressures have been shown to cause basal sliding.

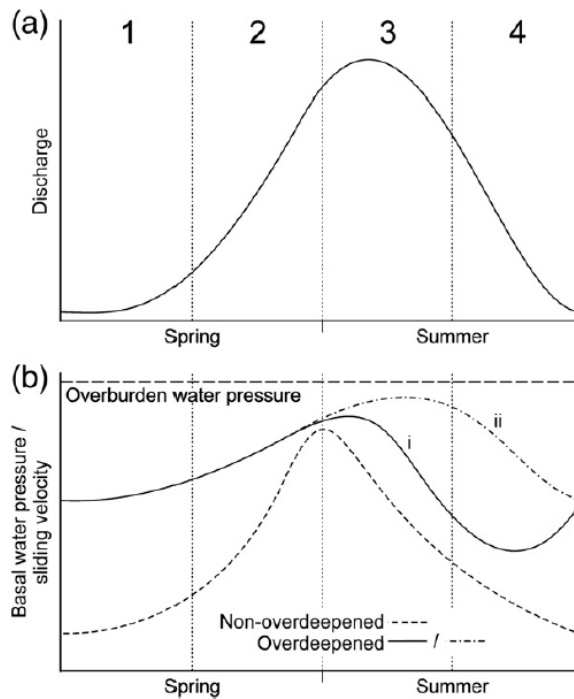


Figure 2: Hypothetic diagram showing a) typical variation of discharge during the ablation season and b) how basal water pressure and sliding velocities could evolve over the ablation season for a non-overdeepened and an overdeepened glacier. In the beginning of the melting season, the discharge rises and without the presence of an overdeepening, the basal water pressure/ sliding velocity increases as well because of the low efficiency to evacuate the rising supply of discharge. The rapid increase continues to the point when a more efficient drainage system has been developed. After this point, water is drained more efficiently and the basal water pressure decreases. For an overdeepened glacier, the basal water pressure in the beginning of the melt season is higher, because of inefficient drainage through the overdeepening. The shifting to a more efficient system could then be expected to be delayed compared to a non-overdeepened glacier (curve i) or not evolve (curve ii). (From Cook and Swift, 2012)

Creyts and Clarke (2010) examined the impact of overdeepenings on the hydraulics of a glacier by a numerical model and concluded that the morphology of an overdeepened system could change diurnally as discharge alters and is depending on the

steepness of the bed.

2.4 HYPOTHESIS

Based on what is known about drainage within overdeepened glaciers, the following hypothesis could be stated:

At Griesgletscher, it is likely that the biggest part of the runoff in the overdeepened area and areas upglacier of the overdeepening does not pass through the overdeepening. Instead it is likely that the discharge is drained via an englacial channel passing over the overdeepening or a lateral channel passing on the outer side of the overdeepening. Without the presence of these channels, the drainage system upglacier from the overdeepening can be expected to have a limited capacity to evacuate water as well.

For a non-overdeepened glacier, the drainage system has been shown to develop during the ablation season from an inefficient, distributed system to a more efficient, channelized system. For Griesgletscher, on the other hand, this evolution can be expected to be delayed or not occur because of the presence of the overdeepening.

3 FIELD CAMPAIGN

Here follows a description of the fieldwork performed at Griesgletscher during the ablation season 2017. First, the field site is introduced followed by a description of the monitoring station and the methods used. In this thesis, left and right is defined in orographic sequence.

3.1 FIELD SITE

The field campaign took place at Griesgletscher, a temperate glacier located in the south of Switzerland, on the boarder to Italy (Figure 3).



Figure 3: Griesgletscher’s location in Switzerland to the left (image retrieved from map.geo.admin.ch). To the right, picture of Griesgletscher taken by Elin Carlsson.

There are three main streams emerging from Griesgletscher and they will in this thesis be called Stream 1, Stream 2 and Stream 3 (Figure 4). Of these, Stream 2 emerging on the right side of the glacier tongue, carries the biggest discharge and joins Stream 1 before reaching the artificial lake, located just under the glacier.

Stream 1 runs only a short distance after having exited the glacier and before joining Stream 2. Stream 3 emerges on the left side of the glacier tongue and carries a small discharge compared to the other streams. Downstream from the glacier a lake is formed by a dam built for hydropower.

The area of Griesgletscher in 2016 was estimated to 4.9 km² and the glacier is situated on an altitude of around 2400 m a.s.l. to 3340 m a.s.l. (Feiger et al., 2018).

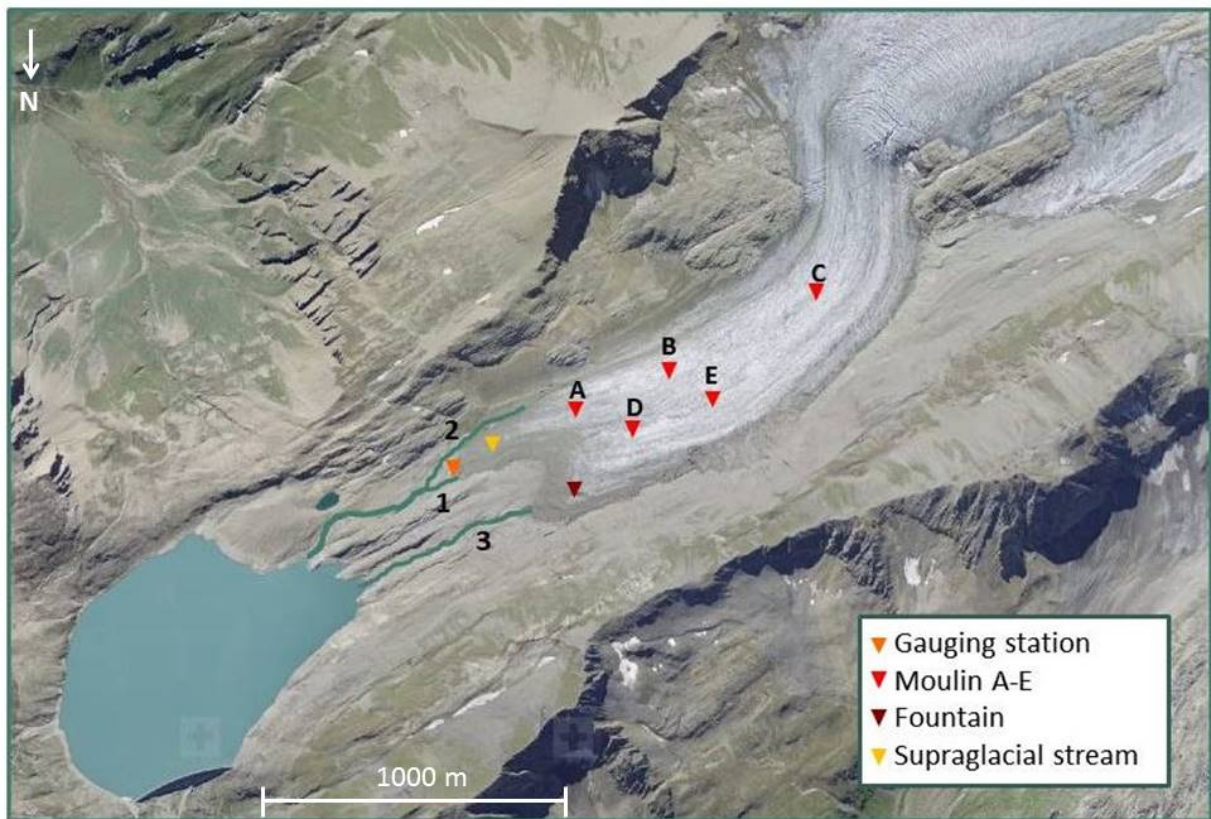


Figure 4: Map over the lower part of Griesgletscher, showing the three emerging streams marked as 1,2,3. Moulin injected in tracer experiments are named A-E. Marked are also the situation of the gauging station, a fountain on the surface of the glacier where dye was detected in one of the tracer experiments and a supraglacial stream that from this position enters the glacier and emerges again in Stream 1 (image retrieved from map.geo.admin.ch).

3.2 GAUGING STATION

A gauging station was installed in Stream 1 in the beginning of the ablation season 2017 (Figure 5). The approximate coordinates for the station were 46 °45'N 8°36'S at an altitude of 2400 m (WGS84). The placement was chosen considering the following criteria: 1) That the water originated subglacially, this was assumed from the high content of sediments that could be observed in the stream, indicating that the discharge had been in contact with the bed under the glacier. 2) The possibility to set up a gauging station, for example a suitable, stable location with sufficient flow. 3) The safety aspect. High erosion causing changes of the fore field could be expected and had to be taken into account when choosing the location for the station.



Figure 5: The gauging station. Photograph: Álvaro Ayala.

The following measurements were made continuously during the ablation season:

- **Turbidity:** measured by two Partech IR15C infra red turbidity sensors (Figure 6 & 7). The turbidity of the water gives an indication of how much suspended sediments the water carries. The turbidity measurements were to be translated into suspended sediment concentration by defining a relationship between TB and SSC calculated from water samples. Two sensors were used, so that in case one got clogged or for other reasons generated uncertain results, measures from the other sensor could still cover this period.
- **Water pressure:** measured by a GE Duck 1800 Pressure transmitter (Figure 6). By monitoring how the water level in the stream varied, the water filled cross section area could be calculated for different times. This, together with results from salt dilution experiments, could then be translated into discharge.
- **Electrical conductivity:** measured by Campbell Scientific 247W probe (Figure 6). EC gives an indication of how fast the water travels through the drainage system, as a longer residence time would allow for more time for chemical reactions to take place, resulting in a higher conductivity (Fenn, 1987).

- **Water temperature:** measured by a thermometer built in the conductivity meter. EC is temperature dependent (Fenn, 1987), and this was compensated for by measuring the water temperature.

Measurements were made every five seconds and stored as five minutes means by a CR10 data logger. A rope put across the stream served as reference for a cross section profile that was measured at every visit in order to evaluate if the bed of the stream changed during the measuring period (Figure 6). At the visits, measurements of existing ablation stakes on the glacier tongue were taken. These results were included in modeling of the discharge performed by Nadine Feiger in the frames of her master project at ETH Zurich.

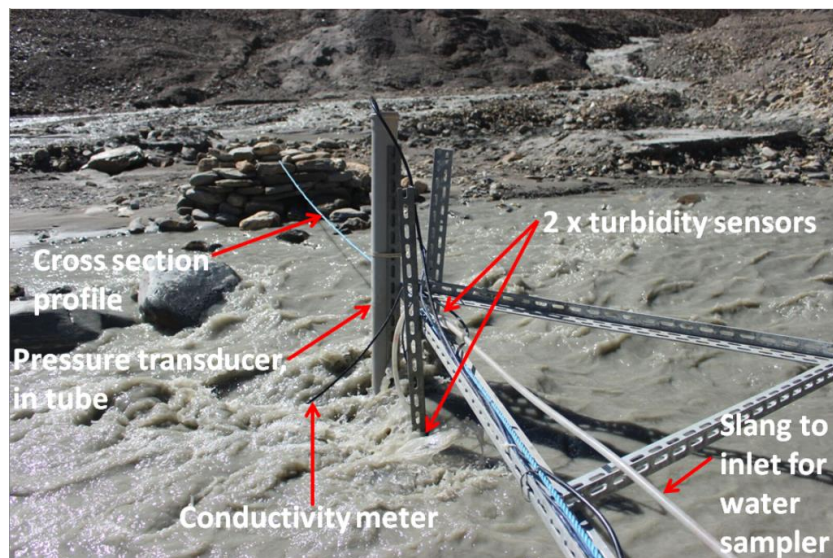


Figure 6: Placement of sensors in the gauging station, picture taken by Álvaro Ayala.



Figure 7: Picture taken during extremely low flow on 07.09.2017 showing the locations of the sensors. Picture by Marie Selenius.

3.2.1 Water samples

Water samples for calibration of the turbidity measurements were collected with an ISCO automatic water sampler (Figure 8). A total of 115 samples of a volume between 200-900 ml were collected and brought back to the laboratory where they were filtered. The filtrates were dried for 24 hours in a temperature of 50 °C and weighed. The suspended sediment concentration was calculated for each water sample. In order to get a representative distribution of suspended sediments at different water levels, the inlet of the water sampler is shaped as a long cylinder, and was put in an angle of about 45 °C (Gomez, 1987) (Figure 7).



Figure 8: Automatic water sampler. Photographs: Álvaro Ayala (left) and Sigrid Björnsdóttir (right).

3.2.2 Salt dilution experiments

By injecting a known quantity of salt into a stream and measuring the conductivity downstream, discharge can be calculated. A total of 39 salt dilution experiments were performed on three occasions spread out over the season (Figure 10) and was translated into discharge by Nadine Feiger in the frames of her master project at ETH Zurich. The calculated discharge could then be related to measured water pressure, in order to find a relationship that could be used to retrieve an hourly series for discharge.

3.2.3 Maintenance

The gauging station was visited and maintained every six to nine days. The regular one day visits for maintenance and collection of data and water samples was extended with a 24 hours measuring campaign in beginning of August (Figure 10). During this campaign, hourly water samples were collected and various tracer experiments performed.

The instruments installed at the gauging station were running between 02.07.2017-07.09.2017. With a break in the first half of August, when a flood event caused a displacement of Stream 1 and the measurements were interrupted until the station

was reinstalled in middle of August (Figure 10). At the visit of the station on 07.09.2017, the runoff had decreased drastically and the sensors were all situated above the water surface (Figure 7). Because of the low water level, it was not possible to find a suitable location for continuation of the monitoring of Stream 1 and the monitoring was interrupted. Data indicates that the water level went down already in end of August, thus useful data extends to this day (Figure 10).

3.3 TRACER EXPERIMENTS

To get a better picture of the drainage systems morphology and how it changed during the season, dye tracing experiments were performed. This was done by injecting dye, Rohdamine WT, in a moulin (Figure 9) and measuring the fluorescence downstream with a fluorometer (10 AU Fluorometer from Turner Design). The time from injection to detection, the travel time, was also noted.

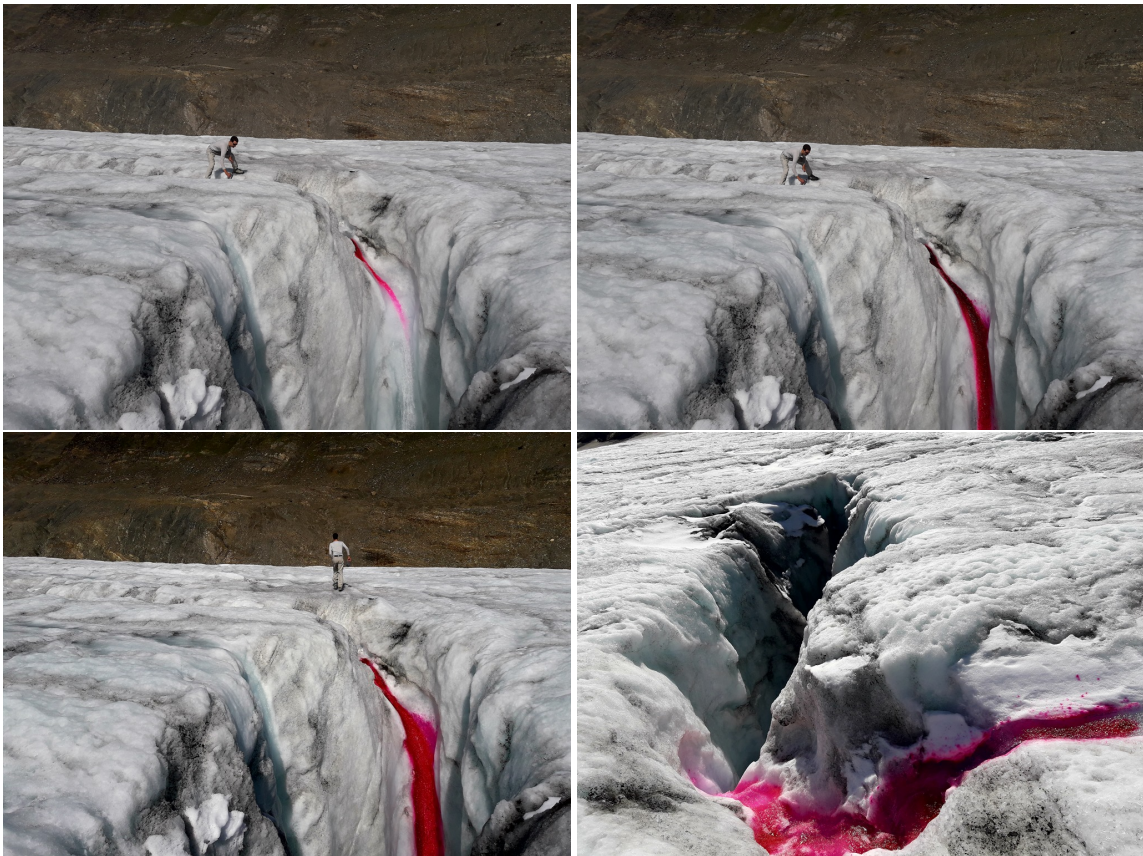


Figure 9: Dye injected in Moulin C on 15.08.2017. Pictures taken by Johannes Landmann

In order to read the fluorescence, water samples were collected manually and were likewise manually injected into the fluorometer. Measurements of fluorescence are sensitive to turbidity and the high concentration of sediments in the stream water disturbed the readings. The collected water samples were therefore left to rest for at least 30 min before reading was done. This allowed for some of the sediments to settle at the bottom of the sample and resulted in more stable readings. Fluorescence is temperature dependent and the resting time before readings also allowed

for the temperature of the water sample to adjust to air temperature. However, the fluorometer had a temperature compensation package that recorded the temperature of the water sample and automatically adjusted the readings. When the water sample had been injected in the fluorometer, three values were noted corresponding to the values showed after 15, 30 and 60 seconds respectively. This as the settling of sediments in the column, still after a resting time, resulted in constantly increasing readings.

The moulins that were injected were chosen after how active they were, i.e. how big the flow of water through the moulin was, and from their location on the glacier. The original plan was to select a small number of moulins and continue to inject these throughout the melting season. Attempts were done to inject the same moulins at the same time of the day so that results for travel time from different injections would be comparable. As the travel time through the glacier could be assumed to depend on the magnitude of discharge, with daily alterations, the time of injection would be likely to affect the travel time (Werder et al., 2010).

3.4 FIELDWORK TIME SCHEME

The performed fieldwork, with visits, experiments and significant events was summarized in a time line (Figure 10).

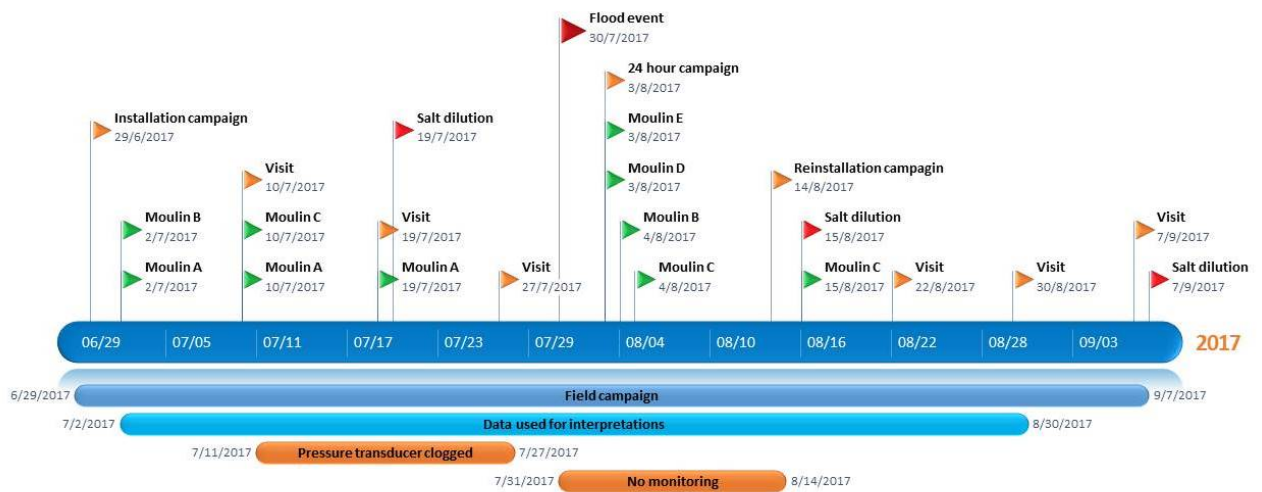


Figure 10: Time line for the field campaign. Marked are visits at the station, days when salt dilution experiments were performed and the approximate time for the flood event. Occasions when tracer experiments were performed are represented by the moulin that was injected. The time line also demonstrates the time period that has been used for regression analysis, containing a gap when 1) the pressure transducer was not working and 2) the time between the flood event and the reinstallation of the station.

4 DATA PROCESSING

Below follows a description of analysis of the data collected during the field campaign. All calculations were made in the R program.

4.1 PREPARATION OF DATA SET

Before starting the analysis, the data set was reviewed and values corresponding to times when the sensors were clogged or above the water level removed. The result left a data set with a gap in the beginning of August, during the time from the flood event until the reinstallation of the station. There is also a gap in the data set for the pressure transducer in July, caused by clogging of the sensor (Figure 10). Short periods of missing values in the water pressure and the EC time series were filled by linear interpolation. Values generated by the two TB sensors were combined into one TB series consisting of the mean from the two sensors at times when they were both monitoring and from one of the sensors at times when the other one was clogged or above water level.

4.2 CALIBRATION OF A TURBIDITY - SUSPENDED SEDIMENT CONCENTRATION RELATION

A log-log linear regression was conducted between SSC, calculated from collected water samples, and corresponding TB measurements (Equation 1, $n=115$, $r^2 = 0.53$) (Figure 11). The relation retrieved is described according to equation 1. R-code is provided in Appendix A.

$$\log SSC = 1.76 + 0.66 \cdot \log TB \quad (1)$$

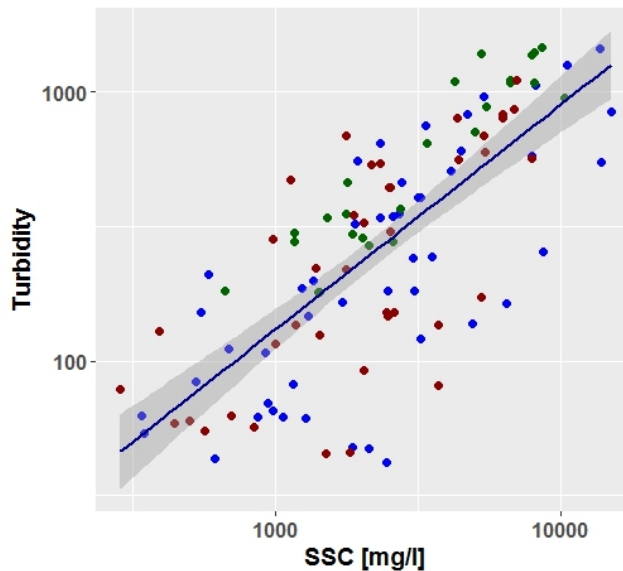


Figure 11: Log-log linear regression for TB measurements and SSC calculated from collected water samples. Blue dots represents samples collected before the flood event, green dots samples collected after the flood event and red dots are manually collected water samples from the 24 hour field campaign. The blue line represents the linear regression with 95% confidence interval. $n= 115$, $r^2 = 0.53$.

The relationship was used to translate TB measurements into a continuous time series of SSC.

4.3 CALIBRATION OF A STAGE - DISCHARGE RELATION

Below follows a description of how hourly discharge data was calculated from field data. The R-code that was used for the calculations is found in Appendix B.

The measurements from the pressure transducer were first translated into a height, representing the water level, WL, in the stream according to Equation 2.

$$WL = h_p + (-1)P_w \cdot 100 \cdot 6.8948/g \quad (2)$$

Where h_p is the height of the pressure transducer above the bed of the stream in meters, P_w is the measures of the pressure transmitter in psi, and g is the gravity, here put to 9.81m/s^2 . As the pressure transducer generated negative values of the pressure above the sensor, the (-1) is needed in order to generate a positive water level. 100 and 6.8948 are conversion factors that are needed as the unit for the pressure transducer is psi.

The cross section profile together with the water level was used to generate a water filled cross section area, A , of the stream. This calculation was done in R for hourly values of the water level (Appendix B). As the cross section profile was measured at every visit of the gauging station, the profile corresponding to respectively time period could be used.

As a next step, the results from the salt dilution experiments were used to calibrate a relationship between discharge and water filled cross section area. Only at one of the three occasions when salt dilution experiments were performed did the pressure transducer work. This was on 15.08.2017 and these measurements were therefore used to perform a linear regression (Equation 3, $n=9$, $r^2 = 0.64$) between water filled cross section area and discharge (Figure 12).

$$Q = -0.60 + 0.83 \cdot A \quad (3)$$

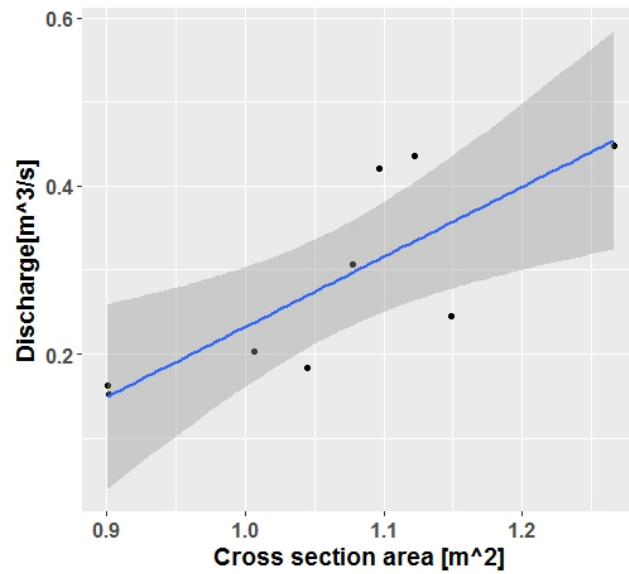


Figure 12: Cross section area plotted against discharge obtained from salt dilution experiments. The blue line represents the fitted regression with a 95 % confidence interval marked in gray. $n=9$, $r^2 = 0.64$.

The salt dilution experiments were made at different times of the day, between 10:00 - 17:00, thus the lowest discharges expected at night and early in the morning were not covered. Equation 3 therefore gives negative discharge values for the lowest water levels. As $Q=0$ would give no water in the cross section, the intercept was assumed to be zero. This derived the following equation ($n=9$, $r^2 = 0.91$):

$$Q = 0.27 \cdot A \tag{4}$$

Equation 4 was finally used to translate water filled cross section area into discharge.

5 RESULTS AND OBSERVATIONS

The results and observations obtained within the field campaign are presented below.

5.1 RESULTS FROM THE GAUGING STATION

After calculation of SSC and Q (Section 4.2 and 4.3) the results could be visualized and compared to weather data (Figure 13; Appendix C). Data for air temperature, global radiation and precipitation were obtained from Meteoschweiz.admin.ch. Robiei, located 11 000 m southwest of Griesgletcher at an altitude of 1900 m a.s.l, was the closest weather station and considered as most representative.

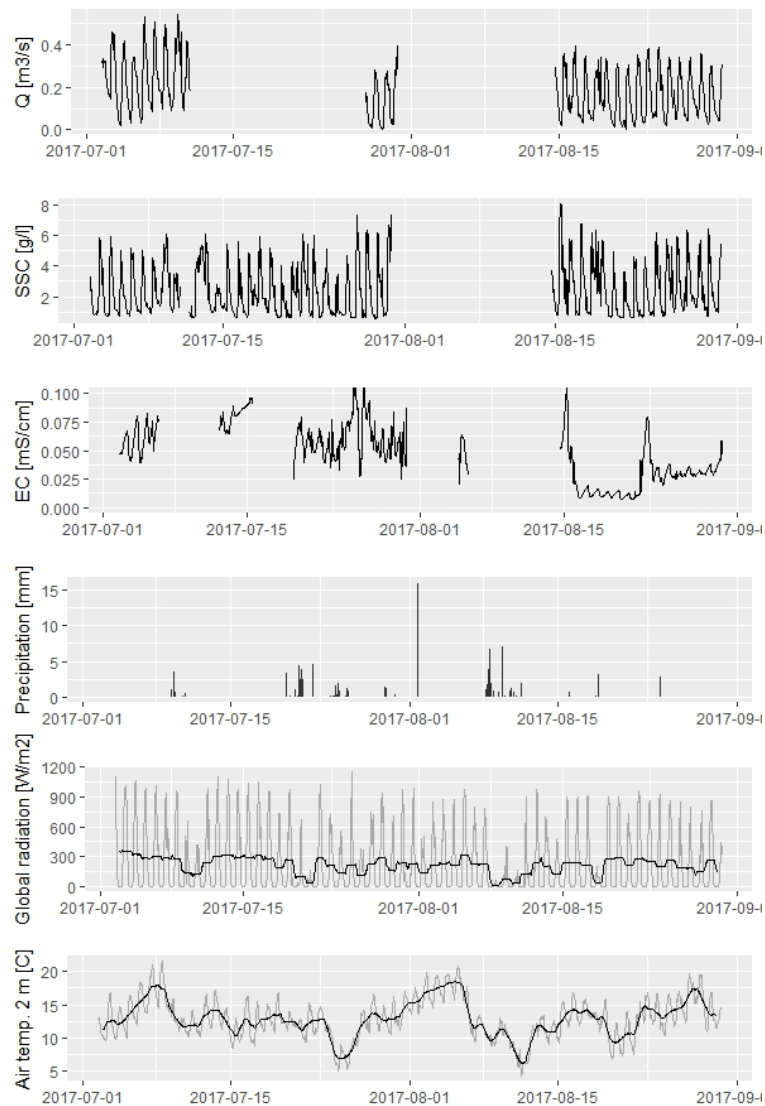


Figure 13: Results from the gauging station and weather data from the weather station Robiei. Data is shown as hourly values. For air temperature and global radiation a 24 hour running mean have been calculated and is represented by the black lines. (Weather data from Meteoschweiz.admin.ch)

A peak precipitation event as well as high temperatures that coincides with the flood event around 01.08.2017 can be noted. A difference in EC can also be observed from

the beginning to the end of the melt season (Figure 13). An interpretation of these observations is provided in Section 8.

5.2 FIELD OBSERVATIONS

Observations at regular visits at the glacier provided some useful insights and knowledge of changes that occurred during the ablation season. Diurnal changes of the amount of runoff were clearly visible to the eye, with high discharge as a result of melt caused by solar radiation and increasing temperatures. At the first visits, big changes in the structure of the glacier surface were observed as a result of increased surface melt and runoff. An increasing amount of active moulins and an overall increased runoff were observed at this time as well. When the gauging station was installed, the turbulent water in Stream 1 indicated subglacial water, while the water colour in Stream 2 was more clear (Figure 14).



Figure 14: Picture of the junction between Stream 1, to the left, and Stream 2, to the right. A difference in water colour and sediment content could be observed between the two streams. Photograph: Marie Selenius.

The most drastic observation that was done in field was a flood event that occurred around 01.08.2017. The flood caused a displacement of Stream 1, so that it no longer passed the gauging station but was relocated a few meters south-west. Leaving the former gauging station with the instruments buried under sediments and rocks (Figure 15).



Figure 15: To the left, picture taken on 15.08.2017 showing the old placement of the gauging station and the new location of Stream 1. To the right, the sensors were completely covered by sediments and rocks after the flood event. Photograph: Marie Selenius.

After the flood event, a change of the water colour of Stream 2 was observed. The colour of the water shifted from being clear to containing a big amount of sediments. From further observations it turned out that the sediment content of the water in Stream 2 would alter in a diurnal cycle, with low concentrations of sediments corresponding to times of low discharge, at night and in the morning, and high concentration of sediments as the discharge increased around noon (Figure 16).



Figure 16: Pictures of Stream 2 taken on 07.09.2017, to the left in the morning and to the right in the afternoon. Photograph: Marie Selenius.

5.3 RESULTS FROM TRACER EXPERIMENTS

A total of ten tracer experiments were performed during the ablation season (Table 1). Of interest was primarily where the dye was detected and the travel time, that is the time from injection to detection. After having estimated the distance from the moulins to the place for detection, a minimum velocity could be calculated. That is to say, the velocity of the discharge if it would travel the shortest way from the location for injection to where it was detected.

Table 1: Summary of the results from performed tracer experiments, the travel time is the time from injection to when the dye was first detected. No detection for measurements done for at least 3 h after injection is marked as $-$. Injections were done in moulins A-E. S1 indicates detection in Stream 1 and S2 detection in Stream 2. F indicates detection in a surface fountain on the left side of the glacier tongue (Figure 4).

| Date | Time of injection | Injection | Detection | Travel time [min] | Minimum velocity [m/s] |
|------------|-------------------|-----------|-----------|-------------------|------------------------|
| 02.07.2017 | 10:30 | M B | S2 | 140 | 0.11 |
| 02.07.2017 | 14:38 | M A | S1 | 89 | 0.11 |
| 10.07.2017 | 11:50 | M C | S2 | 69 | 0.36 |
| 10.07.2017 | 14:55 | M A | S1 | 74 | 0.13 |
| 19.07.2017 | 12:45 | M A | $-$ | $-$ | $-$ |
| 03.08.2017 | 15:58 | M D | F | $-$ | $-$ |
| 03.08.2017 | 18:17 | M E | $-$ | $-$ | $-$ |
| 04.08.2017 | 09:05 | M B | $-$ | $-$ | $-$ |
| 04.08.2017 | 12:45 | M C | $-$ | $-$ | $-$ |
| 15.08.2017 | 10:40 | M C | S1 | 40 | 0.63 |
| 15.08.2017 | 10:40 | M C | S2 | 35 | 0.71 |

The results from the tracer experiments give an indication of how the subglacial drainage system is structured and points out changes of the morphology of the drainage system as the season evolves. In beginning of July, Moulin A gave detection in Stream 1 and Moulin B gave detection in Stream 2. The minimum velocities for the two flows were similar, 0.11-0.13 m/s (Table 1). The fastest velocity, 0.36 m/s, was found for injections in Moulin C, located highest up on the glacier tongue (Figure 4). This suggests that discharge from Moulin C did not pass through the overdeepening, but rather followed an englacial or lateral, more efficient, pathway. On 19th of July, Moulin A was injected, but gave no detection. At the same day, observations on the glacier indicated that this moulin was less active than before. In the beginning of August, Moulin A was no longer active and dye injections in moulin B, C and E gave no detection during the three hours that fluorescence was measured downglacier. Injection in Moulin D gave at the same occasion detection in a surface fountain on the left side of the glacier tongue (Figure 4) suggesting englacial drainage towards Stream 3. On 15th of August, an attempt to inject Moulin C in the beginning of the day, while the water in Stream 2 was still clear, was done and gave detection in both Stream 1 and Stream 2, with two peaks at each location. The results from dye tracing experiments and the locations for the moulins were compared to the bedrock of Griesgletscher. An image of the bedrock (Figure 17) was created in ArcGIS from a digital elevation model obtained from Ground Penetrating Radar measurements (Feiger et al., 2018).

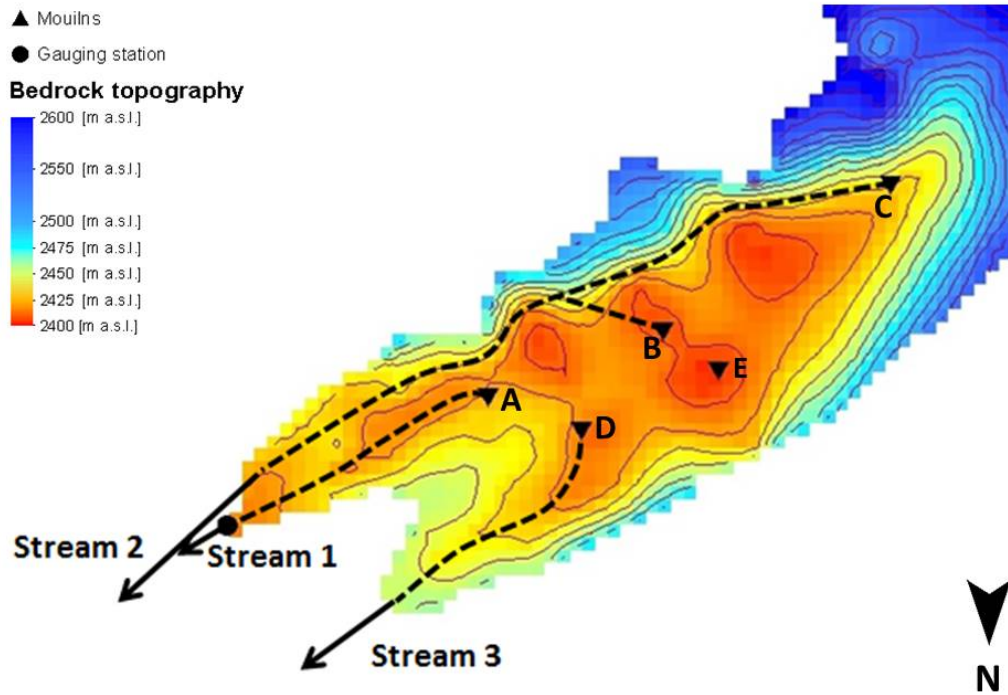


Figure 17: Bedrock for the lower part of Griesgletscher from a model based on GPR measurements done in 2016. Marked are the three streams emerging from the glacier, injected mouilns and the gauging station. Contours represent elevation changes of 15m. Dashed lines are imaginary drainage routes based on interpretation of tracer experiments and field observations (Digital elevation model provided from Nadine Feiger).

5.4 SALT DILUTION EXPERIMENTS

The results from the salt dilution experiments were used for translating measurements of water pressure in Stream 1 into Q (Section 4.3). Moreover, salt dilution experiments were performed on different locations so that Q could be calculated for Stream 1, Stream 2 and the part where Stream 1 and Stream 2 joins together, called Stream 5. The results from the salt dilution experiments were processed by Nadine Feiger and give an indication of the difference in magnitude of Q in Stream 1 and Stream 2 (Figure 18).

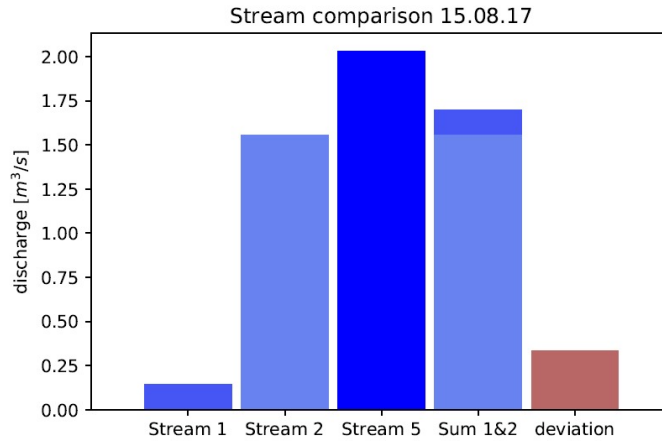


Figure 18: Results for discharge in Stream 1, Stream 2 and Stream 5 performed on 15.08.2017. Stream 5 is the part after the junction of stream 1 and Stream 2. (Diagram produced by Nadine Feiger).

Shortly after the monitoring station, Stream 1 joins Stream 2. Q after the junction should therefore be equal to the sum of Q in Stream 1 and Stream 2. However, the results give an idea of the difference in magnitude of Q between Stream 1 and Stream 2 and also a hint of how big deviation that can be expected from the salt dilution experiments (Figure 18).

Salt was also injected in a supraglacial stream, just above Stream 1, that by tracer experiments had been established to emerge in Stream 1 (Figure 4). This, to evaluate the portion of subglacial water in Stream 1 (Figure 19).

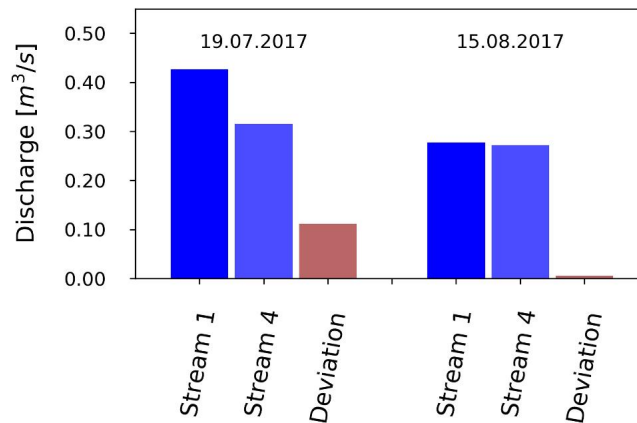


Figure 19: Result from salt dilution experiments performed at 19.07.2017 and 15.08.2017, showing the discharge in Stream 1 and also discharge measured in the supraglacial stream, in the figure called Stream 4, that from dye tracing experiments was determined to emerge Stream 1. (Diagram produced by Nadine Feiger).

The result suggests that only a small portion of the discharge in Stream 1 have subglacial origin (Figure 19).

6 SUSPENDED SEDIMENT CONCENTRATION AND DISCHARGE

The relation between SSC and Q can reveal important information about drainage morphology (Willis et al., 1996; Hodgkins, 1999; Hodson and Ferguson, 1999; Swift et al., 2005). The relationship was analyzed using simple linear regression and thereafter by multiple linear regression, evaluating the influence of various explanatory variables. All analysis were made in the R program. The process follows mainly the approach described by Swift et al. (2005) in their study at Haut glacier d’Arolla.

6.1 LINEAR REGRESSION

The relationship between SSC and Q was analyzed using simple linear regression, R-code is found in Appendix D. Presented below is first some theory for linear regression, followed by the course of action for the analysis and finally the results obtained.

6.1.1 Theory

The general form for a simple linear regression can be described as follows:

$$Y = \beta_0 + \beta_1 X_1 + \epsilon \quad (5)$$

where Y represents the dependent variable, in this case $\log SSC$. X_1 represents the explanatory variable, here $\log Q$, and β_1 its coefficient, i.e. the gradient of the relationship. β_0 describes the intercept with the y-axis and ϵ is a random variable representing the variance not explained by the model (Helsel and Hirsch, 1993). The residual, e_i , for response variable i represents the deviation between observed, Y_i , and fitted, \hat{Y}_i , values (Equation 6).

$$e_i = Y_i - \hat{Y}_i \quad (6)$$

In the R program, a summary of the statistics is provided for each regression. Considered was, inter alia, the r^2 -value describing the fraction of variance of SSC explained by the regression. For each coefficient, β , the uncertainty is also provided as the standard error, SE. A 95 % confidence interval, CI, could be calculated for each coefficient according to (Equation 7) (Helsel and Hirsch, 1993).

$$CI = \beta \pm 2SE \quad (7)$$

Two coefficients are said to be significantly different if their confidence intervals do not overlap. That is to say, they are statistically different at the 95% confidence level (Helsel and Hirsch, 1993).

By describing a relationship from a linear regression, some assumptions are made about the residuals. These are that the residuals are independent, normally distributed and that the variance of these is constant (Helsel and Hirsch, 1993) and thus does not change depending on the discharge or over time. Residuals that fulfill

these criteria would show a random noise, i.e. no visible patterns. When examining how the residuals change over time, serial autocorrelation can indicate if the time series contain shorter periods of trends or correlation, which would oppose the assumption made when performing linear regression. Thus, analysis of the residuals makes an important part when examining the suitability of a regression.

6.1.2 Transformation of the data

Before conducting regression analysis, the data was visualized (Figure 20). It appears that the variance increases as discharge increases, thus a log transformation was considered. A log-transformation is suitable for 1) variables that do not take negative values and 2) if the variance of the residuals increases for increased values of the variable. The log-transformation has also been successfully used for SSC and Q in previous studies (Swift et al., 2005).

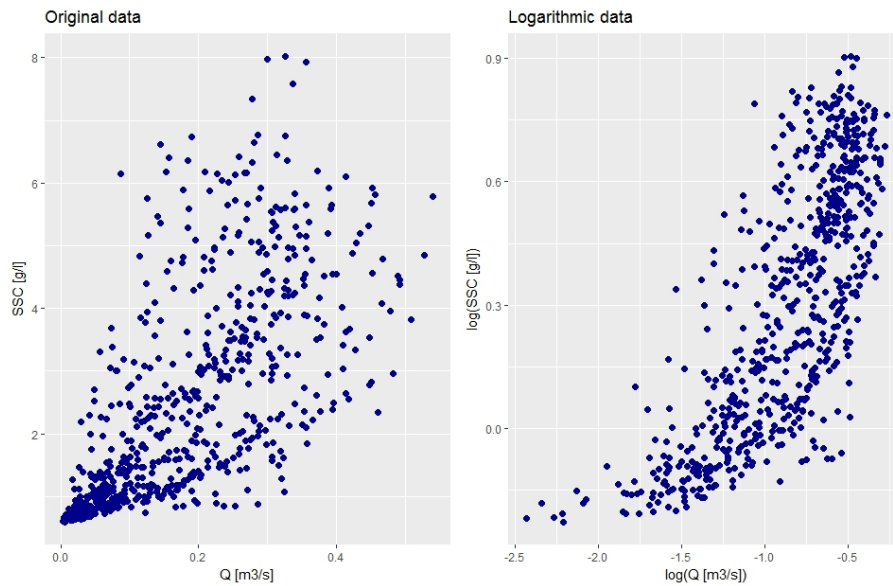


Figure 20: SSC plotted against Q to the left and log-transformed series to the right. Including all data available between 02.07.2017 - 30.08.2017.

A log transformation of SSC and Q seems to be better explained as a linear relationship than non-transformed data (Figure 20) and was considered as more suitable to use for linear regression.

6.1.3 Approach

A log-log linear regression for SSC against Q was made for hourly data available for the beginning of July ($n=202$, $r^2=0.535$) and for the end of August ($n=360$, $r^2=0.635$) (Figure 10). In order to evaluate time dependence in the residuals, these were plotted over time (Figure 21).

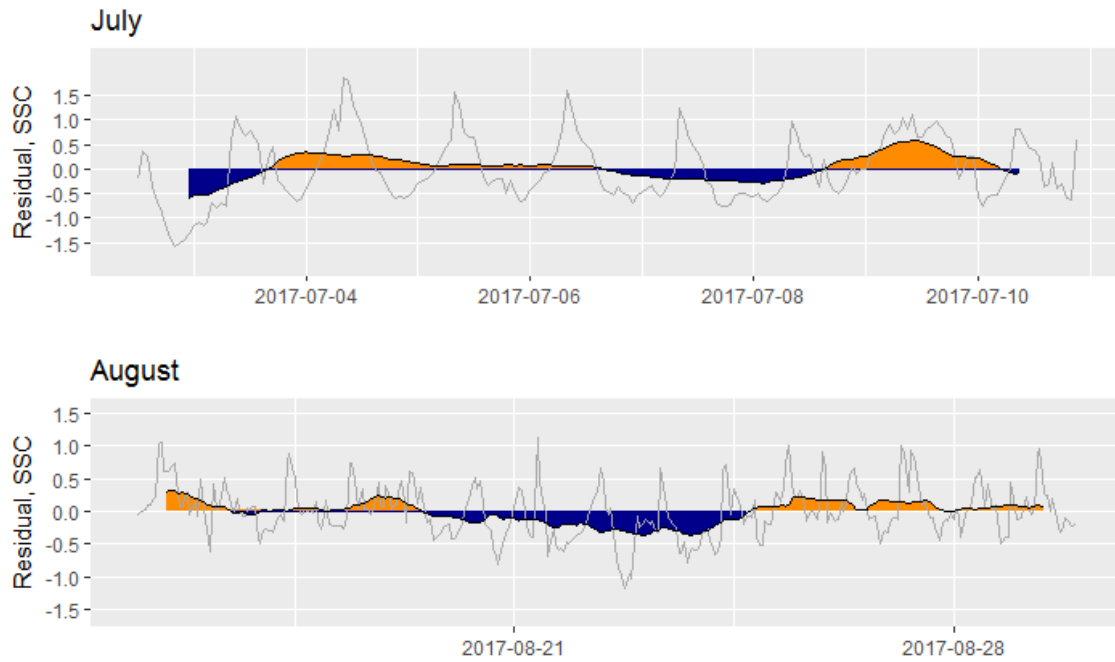


Figure 21: Residuals for SSC achieved from the log-log linear regression between SSC and Q for data from July (02.07.2017 - 10.07.2017) and August (15.08.2017 - 29.08.2017). The regression was done for hourly mean values and the residuals are represented by the gray line. The black line represents a 24 hour running mean, while the orange and blue fields represents areas of positive and negative residuals respectively.

Given that the residuals for SSC show the deviation between measured and fitted values, periods for which the SSC is overestimated respectively underestimated by the linear regression could be identified (Figure 21). Periods for which the residuals are > 0 represents periods when the turbidity is underestimated and indicates that the gradient of the relationship between SSC and Q was increasing at this time. The gradient of the relationship gives in turn an indication of how efficient the drainage system is to evacuate suspended sediments. Thus, this would mean that the efficiency to evacuate suspended sediments was increasing during periods for which residuals are > 0 . Similarly, periods for which the residuals are < 0 represents periods of overestimated SSC and indicates that the gradient for the relationship between SSC and Q was decreasing. Which suggests that the efficiency to evacuate suspended sediment was decreasing. This suggests that the relationship between SSC and Q was changing over the season, causing autocorrelation in the SSC residuals and proposes a division of the data set into subperiods. The goal of such division would be to identify short term trends and to represent these in individual subperiod. For this cause, the behavior of the SSC - Q relation needed further examination.

6.1.4 Moving window regression

To find the most suitable subperiods, representing short term trends, the relationship between Q and SSC was further investigated by conducting a moving window regression for different window sizes. Thus, linear regression was performed for sub-

periods of lengths between one and ten hours, one at the time. For each length of subperiod, a regression was conducted starting at the beginning of the time period, performing one linear regression for the length of interest, then moving one day ahead and performing a new regression. The coefficients obtained from the regressions, that is the intercepts, β_0 and gradients of the relation between SSC and Q , β_1 , were then plotted over time (Figure 22). R-code is provided in Appendix E.

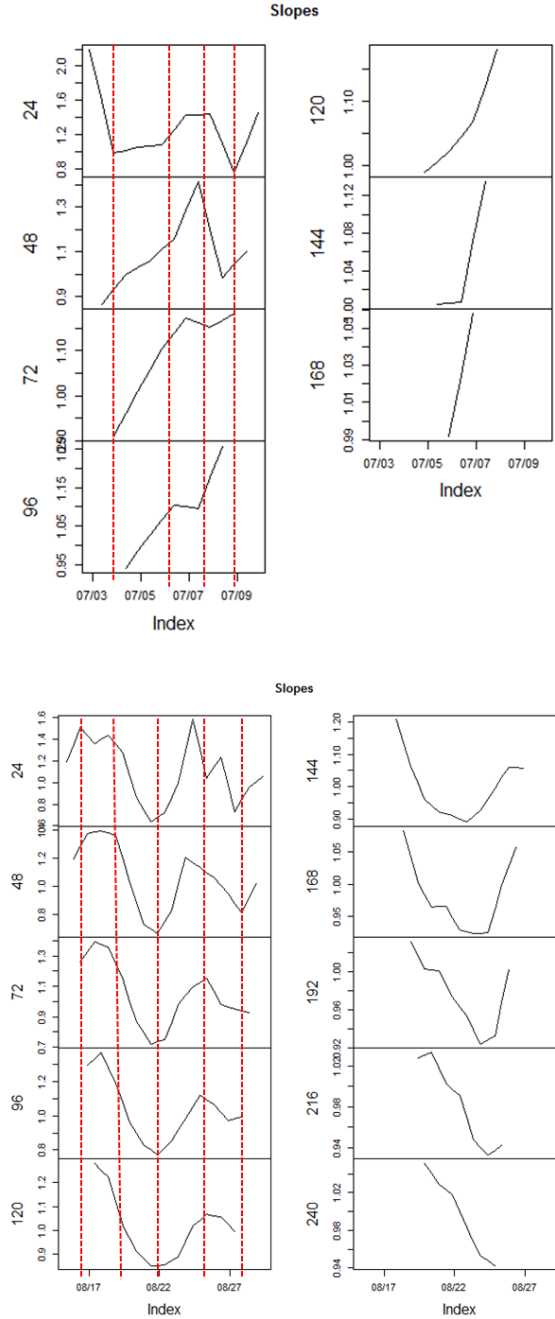


Figure 22: Results for β_1 , or slopes, obtained from moving window linear regression for July above and August below. Red lines marks examples for where changes in the relationship between $\log SSC$ and $\log Q$ seems to occur and served as reference when subperiods were defined. The length of the subperiods for each window is indicated in hours on the left side of the panels.

Visualization of how gradients altered for different possible lengths of subperiods gave an indication for how to define representative subperiods. Changes of the intercept were analyzed following the same approach as for the gradients and showed similar patterns (Appendix F).

6.1.5 Subperiods

Subperiods covering short term trends could be identified based on residual analysis (Figure 21) and moving window regression (Figure 22). Different combinations of subperiods were investigated in order to find subperiods that to the greatest extent reduced residuals and increased the amount of variance of SSC explained by the linear regression between $\log SSC$ and $\log Q$. Beyond the data that has earlier been examined, available data for SSC and Q allowed for one additional subperiod in end of July (27.07.2017-30.07.2017). Because of the short interval, this was left as one subperiod without further investigation of subdivision.

Defined subperiods are given in Table 2.

Table 2: Subperiods defined for July and August. The r^2 value represents the portion of variance of SSC explained by the linear regression performed for individual subperiods and n indicates number of hours.

| Period | n | Days | Interval | r^2 |
|--------|-----|------|---------------------------------|-------|
| JSP1 | 24 | 1 | 02.07.17 12:00 - 03.07.17 11:00 | 0.511 |
| JSP2 | 72 | 3 | 03.07.17 12:00 - 06.07.17 11:00 | 0.630 |
| JSP3 | 106 | 4.4 | 06.07.17 12:00 - 10.07.17 21:00 | 0.598 |
| JSP4 | 74 | 3 | 27.07.17 15:00 - 30.07.17 16:00 | 0.559 |
| ASP1 | 24 | 1 | 15.08.17 00:00 - 15.08.17 23:00 | 0.784 |
| ASP2 | 84 | 3.5 | 16.08.17 00:00 - 19.08.17 11:00 | 0.579 |
| ASP3 | 84 | 3.5 | 19.08.17 12:00 - 22.08.17 23:00 | 0.665 |
| ASP4 | 48 | 2 | 23.07.17 00:00 - 24.08.17 23:00 | 0.793 |
| ASP5 | 120 | 5 | 25.08.17 00:00 - 29.08.17 23:00 | 0.712 |

When the subperiods had been defined, linear regression could be conducted for each subperiod and the residuals for SSC visualized (Figure 23).

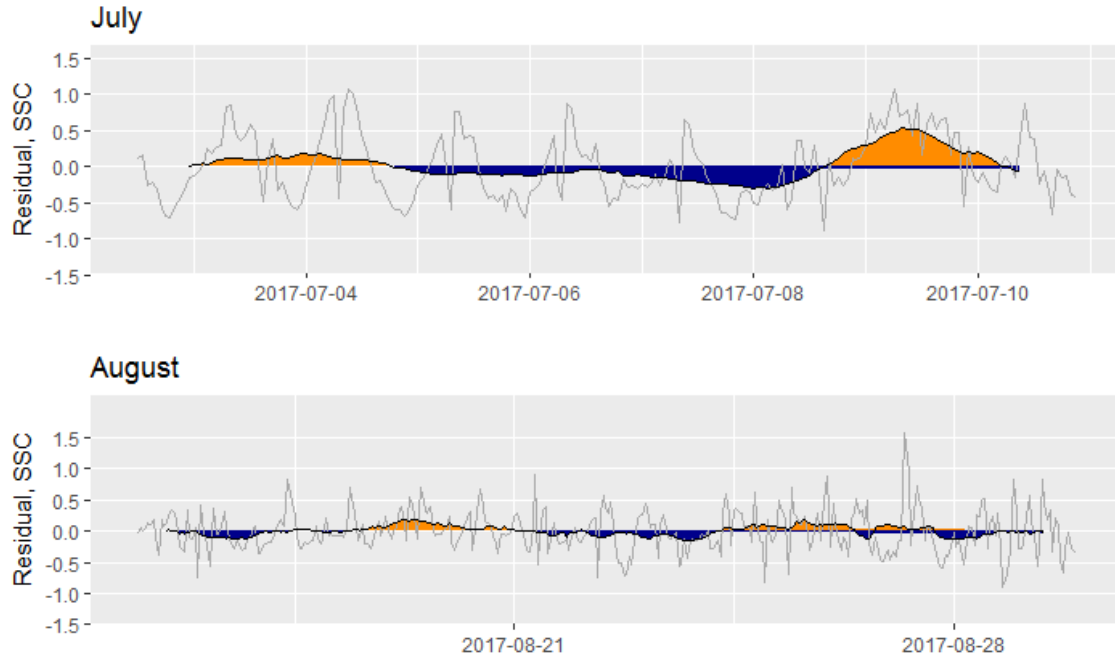


Figure 23: Residuals for SSC from log-log linear regression after that the data was divided into three subperiods for July and five subperiods for August. The regression was done for hourly mean values and the residuals are represented by the gray line. The black line represents a 24 hour running mean, while the orange and blue fields represents areas of positive and negative residuals respectively.

Subdivision has successfully reduced residuals for August, even if some autocorrelation still seems to be present. For July, on the other hand, subdivision did not succeed in reducing autocorrelation and a period of notable overestimation remains at the end of the period. For the range of possible subperiods that were examined for July, no combination resulted in decreased residuals. The result will be further discussed in Section 8.

6.1.6 Results

Linear regression was conducted for defined subperiods (Table 2). The time lag between $\log SSC$ and $\log Q$ that for each subperiod gave the strongest correlation was defined using the cross correlation function in R. Results showed that a one hour lag between the series gave the strongest correlations for most subperiods, so that $\log SSC_t$ corresponded to $\log Q_{t+1}$. New linear relationships were calculated for each subperiod including the calculated lags. This gave relationships that, in most cases, explained more of the variance of SSC than for non-lagged relationships.

The coefficients obtained from the linear regression analysis can be used for interpretations of the drainage system's mechanisms and evolution. The gradient of the relationship (β_1) gives an indication of the drainage systems capacity to evacuate suspended sediments. High β_1 suggests that the capacity to evacuate suspended sediment is high and vice versa. The intercept (β_0), on the other hand, represents the relative availability of suspended sediments. Thus, by visualizing the linear models obtained from individual subperiods, the relationship between SSC and Q could be

further examined. The linear relationships obtained for each subperiod were plotted over the range of discharge that had been measured for every subperiod respectively (Figure 24).

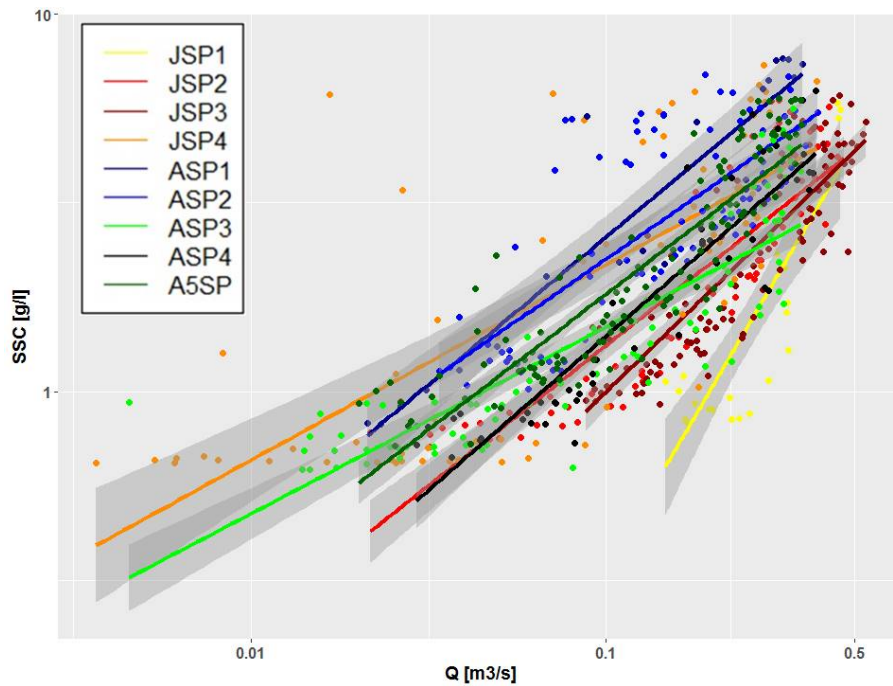


Figure 24: SSC – Q relationships for subperiods defined in Table 2, plotted over the range of discharge measured for every subperiod. The relationships are shown as lines with a 95% confidence interval in gray. The data points from individual subperiods are also plotted as points. The gradient of the lines (β_1) represents the capacity to evacuate suspended sediments and the intercept (β_0) gives an indication of how much sediments that was available during each subperiod. The length of the lines represents the range of discharge observed for each subperiod.

From studies of Figure 24, two distinct subperiods could be identified. That is JSP4 and ASP3. For these periods, the range of discharge observed is wider, including lower minimum discharges. However, studying the distribution of the data for ASP3, the divergent behavior seems to have been caused by solely one point of low discharge. Considering the problems with clogging of sensors and the chance of the water level falling below the level of the sensor, this data point is likely to be an outlier. Exclusion of this point resulted in coefficients for ASP3 that more resembled to other subperiods (Figure 25). Thus, this point was treated as an outlier and excluded. For JSP4, on the other hand, the regression seems to be more representative for the subperiod.

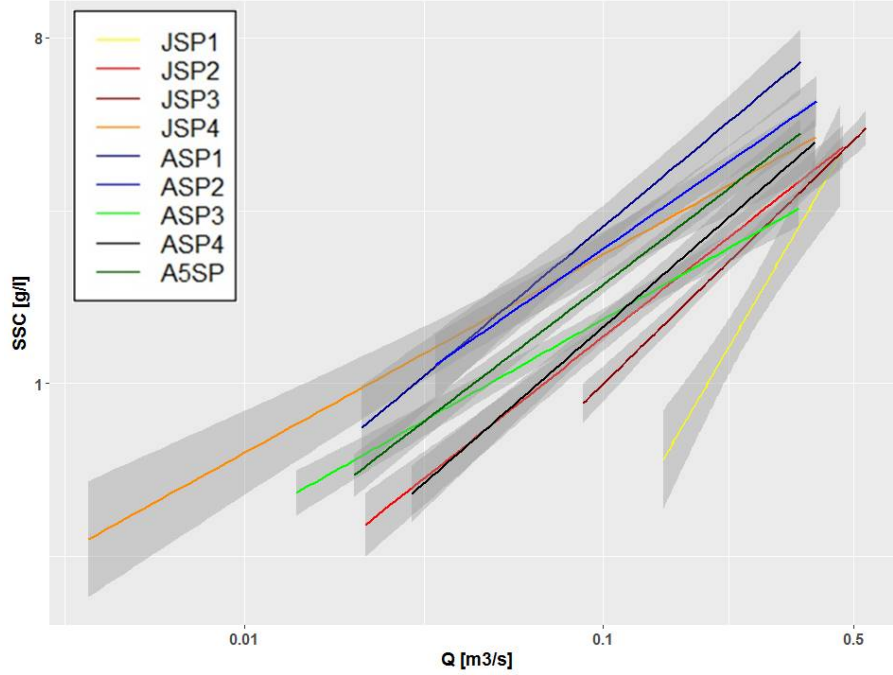


Figure 25: SSC – Q relationship for different subperiods, plotted over the range of discharge measured for respective subperiod. The relationship are shown as lines with a 95% confidence interval in grey. The possible outlier in ASP3 has been excluded.

At last, the result from the linear regression analysis for individual subperiods was summarized and coefficients between different subperiods were compared (Table 3).

Table 3: Results from linear regression. For relations including lag, the lag is specified in hours followed by the correlation obtained. The standard error for the coefficients is marked as SE and confidence intervals calculated as coefficients $\pm 2SE$.

| Period | n | lag [h] (correlation) | Gradient [Confidence interval] | Intercept [Confidence interval] | SE gradient | SE Intercept | r^2 |
|--------|-----|--------------------------|-----------------------------------|------------------------------------|-------------|--------------|-------|
| JSP1 | 24 | 1 (0.746) | 1.610 [1.171 2.049] | 1.420 [1.152 1.410] | 0.220 | 0.134 | 0.710 |
| JSP2 | 72 | 1 (0.865) | 0.742 [0.651 0.834] | 0.864 [0.782 0.947] | 0.0458 | 0.0413 | 0.790 |
| JSP3 | 106 | 1 (0.853) | 0.913 [0.808 1.0182] | 0.912 [0.842 0.912] | 0.0527 | 0.0349 | 0.743 |
| JSP4 | 74 | 1 (0.853) | 0.588 [0.506 0.670] | 0.929 [0.825 1.033] | 0.0410 | 0.0519 | 0.744 |
| ASP1 | 24 | 1 (0.960) | 0.783 [0.657 0.908] | 1.193 [1.064 1.322] | 0.0628 | 0.0644 | 0.876 |
| ASP2 | 84 | 1 (0.815) | 0.690 [0.582 0.798] | 1.033 [0.936 1.131] | 0.0540 | 0.0489 | 0.665 |
| ASP3 | 83 | 1 (0.869) | 0.531 [0.468 0.594] | 0.699 [0.627 0.770] | 0.0316 | 0.0358 | 0.777 |
| ASP4 | 48 | 1 (0.902) | 0.818 [0.718 0.918] | 0.966 [0.871 1.061] | 0.0500 | 0.0477 | 0.853 |
| ASP5 | 120 | 1 (0.885) | 0.718 [0.651 0.785] | 0.977 [0.912 1.042] | 0.0336 | 0.0324 | 0.795 |

Comparing the coefficients obtained from different subperiods, the gradient and the intercept of the relationship between $\log SSC$ and $\log Q$ are in most cases not significantly different from each other. However, JSP1 exhibits a significantly higher gradient than all other subperiods and JSP3 show a significantly higher gradient compare to subperiods JSP4, ASP3, ASP4 and ASP5. Furthermore, a significantly lower gradient and intercept were obtained for ASP3. JSP4 exhibit a lower intercept than JSP3 and ASP4 and ASP1 a higher intercept than JSP2, JSP3, ASP3 and

ASP4. Recalling that the gradient of the SSC-Q relation represents the capacity to evacuate sediments, this suggests that the efficiency to evacuate sediments was lowest during ASP3. Furthermore, the lower intercept obtained for this subperiod indicates a lower relative availability of suspended sediments. The result indicates further that the efficiency to evacuate suspended sediment was highest during JSP1. However, no tendency of seasonal evolution can be seen (Table 3). What implications this could have on the morphology and evolution of the drainage system is further discussed in Section 8. In general, subdivision in combination with the inclusion of time lags increased the portion of variance explained by the regression models. However, to be kept in mind is that the r^2 -value depends on the amount of data included in the regression and that the increase partially could be due to that smaller number of data points are included in the models after subdivision.

6.2 MULTIPLE LINEAR REGRESSION

Residual analysis from linear regression of subperiods indicates autocorrelation. Previous studies suggest that the concentration of suspended sediments, except from discharge, also depends on additional variables. This was investigated by multiple regression analysis. R-code is found in Appendix G.

6.2.1 Theory

Autocorrelation in the residuals may be caused from other reasons than a time dependence. If the dependent variable depends on more than one explanatory variable, but is explained from a simple linear regression, this might cause autocorrelation in the residuals. By performing a multiple regression, the dependent variable is described from several explanatory variables with the goal to find the simplest model explaining as much of the variance as possible, and finally to reduce autocorrelation in the residuals. The general form for a multiple regression can be described as following:

$$Y = \beta_0 + \beta_1 X_1 + \beta_2 X_2 + \dots + \beta_k X_k + \epsilon \quad (8)$$

Similarly as for linear regression, Y represents the response variable. $X_{1:k}$ represents k different explanatory variables and $\beta_{1:k}$ the coefficient for each variable respectively. β_0 describes the intercept with the y -axis and ϵ is the variance not explained by the model (Helsel and Hirsch, 1993).

When including new explanatory variables in a model, consideration must be done to whether the explanatory power added from the variable exceeds the cost. Furthermore, the r^2 -value should be considered with caution as it will increase with every added variable no matter if this variable contributes to a model that better explains the variance of the dependent variable or not. For multiple regression, the adjusted r^2 -value, r_a^2 , that takes into account the least square error and the number of degrees of freedom, represented by the amount of data minus the amount of explanatory variables, therefore gives a better indication of the models explanatory degree. Another point to consider when working with various explanatory variables is multi-collinearity. If two variables explain the same phenomenon, one might be excluded without reducing the models power of explanation (Helsel and Hirsch, 1993).

6.2.2 Approach

Multiple linear regression models were developed by backward elimination, starting off by including all explanatory variables and thereafter excluding the less important, one by one, until only significant variables ($p < 0.05$) remained. Considered was also whether a model including more parameters would explain a bigger portion of the dependent variable or not.

6.2.3 Explanatory variables

Explanatory variables that in previous studies have been shown to be important for explaining the suspended sediment concentration were included in the model (Willis et al., 1996; Hodgkins, 1999; Hodson and Ferguson, 1999; Swift et al., 2005). These are the explanatory variables that were included in the multiple regression analysis:

- **Hours since sub-period began (h).** This variable was included to represent trends within subperiods (Willis et al., 1996; Hodgkins, 1999; Swift et al., 2005).
- **Rate of change of discharge per hour, over the preceding 2 h ($\Delta \log Q$)**
This variable was calculated by subtracting logarithmed values for the mean discharge of the previous two hours from current discharge records. This resulted in a variable with positive values when discharge rises and negative values when discharge declines, thus representing the difference in sediment availability during rising and falling discharge (Willis et al., 1996; Hodgkins, 1999; Hodson and Ferguson, 1999; Swift et al., 2005).
- **Hours since discharge was equalled or exceeded (h_{EE})**
As it is likely that the availability of suspended sediments depends on how much sediments that has already been evacuated by previous discharge, the time that has passed since the discharge was of similar magnitude as the current could be expected to affect the availability of suspended sediments (Willis et al., 1996; Hodgkins, 1999; Hodson and Ferguson, 1999; Swift et al., 2005).
- **Precipitation in the preceding 1,2,3,4 and 6 h, at lags 1-3 h ($\sum P1_{t-0}^{t-0} - \sum P6_{t-3}^{t-0}$).**
Rainwater falling on the sides of the valley will most likely bring sediments when flowing towards the glacier, thus contributing to the suspended sediment availability (Willis et al., 1996). A sum of the precipitation during 1,2,3,4 and 6 hours was included as well as 1-3 hours lags, following the approach of Swift et al. (2005).

Another variable that in previous studies have shown to affect the concentration of suspended sediments is the previous concentration of suspended sediments. Hodson and Ferguson (1999) suggested that a reason for this could be that a higher velocity of the water is required to lift sediment from the bottom, than is needed to keep the sediments suspended. Swift et al. (2005) stated that inclusion of the

sediment concentration in the previous hour, SSC_{t-1} reduced serial autocorrelation in the residuals of SSC in their study at Haut Glacier d’Arolla. Furthermore, when included, SSC_{t-1} showed to be to most significant variable (Swift et al., 2005).

6.2.4 Results

The final models are summarized in Table 4. An interpretation of the results is found in Section 8. In the models, SSC is represented by TB.

Table 4: Results from multiple regression. p-values are indicated as *** ($p < 0.001$), ** ($p < 0.01$), * ($p < 0.05$)

| Period | Equation | | | | | | r_a^2 |
|--------|---------------------|----------------------------------|---|--|---|---|---------|
| JSP1 | $\log(\text{TB}) =$ | 6.799 [5.757 7.841] *** | + | $1.334 \cdot \log Q_{t+1}$ [0.602 2.070] ** | + | $6.621 \cdot \Delta \log Q$ [3.890 9.352] *** | 0.873 |
| JSP2 | $\log(\text{TB}) =$ | 6.972 [6.718 7.225] *** | + | $0.910 \cdot \log Q_{t+1}$ [0.785 1.035] *** | + | $1.945 \cdot \Delta \log Q$ [1.387 2.504] *** | 0.873 |
| JSP3 | $\log(\text{TB}) =$ | 6.903 [6.673 7.133] *** | + | $0.987 \cdot \log Q_{t+1}$ [0.842 1.132] *** | + | $2.725 \cdot \Delta \log Q$ [2.124 3.325] *** | 0.861 |
| JSP4 | $\log(\text{TB}) =$ | 7.675 [7.371 7.980] *** | + | $0.851 \cdot \log Q$ [0.748 0.955] *** | + | $0.733 \cdot \Delta \log Q$ [0.242 1.223] ** | 0.832 |
| ASP1 | $\log(\text{TB}) =$ | 8.681 [8.346 9.016] *** | + | $1.281 \cdot \log Q_{t+1}$ [1.146 1.416] *** | - | $0.106 \cdot \sum P6$ [-0.161 -0.050] ** | 0.940 |
| ASP2 | $\log(\text{TB}) =$ | 10.503 [9.951 11.0541] *** | + | $1.481 \cdot \log Q$ [1.382 1.561] *** | + | $1.662 \cdot \Delta \log Q$ [1.421 1.901] *** | 0.932 |
| ASP3 | $\log(\text{TB}) =$ | 7.265 [6.765 7.765] * | + | $0.773 \cdot \log Q_{t+1}$ [0.677 0.870] *** | + | $0.344 \cdot \Delta \log Q$ [0.117 0.571] ** | 0.804 |
| ASP4 | $\log(\text{TB}) =$ | 7.514 [7.216 7.811] *** | + | $1.133 \cdot \log Q$ [0.999 1.268] *** | + | $3.268 \cdot \Delta \log Q$ [2.382 4.154] *** | 0.890 |
| ASP5 | $\log(\text{TB}) =$ | 9.041 [8.540 9.542] *** | + | $1.087 \cdot \log Q_{t+1}$ [0.991 1.183] *** | + | $0.631 \cdot \Delta \log Q$ [0.381 0.631] *** | 0.819 |

The impact of previous suspended sediment concentration was further evaluated by including an explanatory variable representing the suspended sediment concentration for the previous hour, or in this case the turbidity measured in the previous hour (TB_{t-1}), in the models (Table 5).

Table 5: Results from multiple regression including TB_{t-1} . p-values are indicated as *** ($p < 0.001$), ** ($p < 0.01$), * ($p < 0.05$)

| Period | Equation | | | | | | | r_a^2 | |
|--------|--------------|---------------------------------|---|--|---|--|---|---|-------|
| JSP1 | $\log(TB) =$ | 5.845 [4.680 7.009] *** | + | 0.878 $\log Q_{t+1}$ [0.125 1.631] * | + | 4.329 $\Delta \log Q$ [1.832 6.826] ** | + | 0.00131 $\log TB_{t-1}$ [0.000528 0.00210] ** | 0.862 |
| JSP2 | $\log(TB) =$ | 2.615 *** | + | 0.225 $\cdot \log Q_{t+1}$ ** | + | 2.201 $\cdot \Delta \log Q$ *** | + | 0.583 $\cdot \log TB_{t-1}$ *** | 0.950 |
| JSP3 | $\log(TB) =$ | 6.038 [5.692 6.384] *** | + | 0.618 $\cdot \log Q_{t+1}$ [0.444 0.792] *** | + | 2.473 $\cdot \Delta \log Q$ [1.951 2.995] *** | + | 0.0317 $\cdot \sum P6$ [0.00588 0.0575] * + 0.00101 $\cdot \log TB_{t-1}$ [0.000680 0.00135] *** | 0.898 |
| JSP4 | $\log(TB) =$ | 6.568 [6.079 7.050] *** | + | 0.596 $\cdot \log Q$ [0.468 0.725] *** | + | 0.823 $\cdot \Delta \log Q$ [0.412 1.234] *** | - | 0.0585 $\cdot \sum P6_{t-3}$ [-0.0839 -0.0585] ** + 0.000959 $\cdot \log TB_{t-1}$ [0.000598 0.00133] *** | 0.882 |
| ASP1 | $\log(TB) =$ | 7.557 [5.867 9.247] *** | + | 1.130 $\cdot \log Q_{t+1}$ [1.066 1.194] *** | - | 0.108 $\cdot \sum P6$ [-0.163 -0.0522] ** | + | 0.101 $\cdot \sum P4_{t-1}$ [0.0374 0.165] ** + 0.138 $\cdot \log TB_{t-1}$ [-0.0651 0.340] p > 0.05 | 0.942 |
| ASP2 | $\log(TB) =$ | 10.919 [9.675 12.164] *** | + | 1.507 $\cdot \log Q$ [1.340 1.674] *** | + | 1.184 $\cdot \Delta \log QQ$ [0.927 1.442] *** | + | 0.0325 $\cdot \sum P6_{t-3}$ [0.00991 0.0545] ** - 0.0164 $\cdot \log TB_{t-1}$ [-0.145 0.112] p > 0.05 | 0.926 |
| ASP3 | $\log(TB) =$ | 3.561 [2.660 4.461] *** | + | 0.350 $\cdot \log Q_{t+1}$ [0.231 0.469] *** | + | 0.555 $\cdot \Delta \log Q$ [0.388 0.723] *** | + | 0.638 $\cdot \log TB_{t-1}$ [0.502 0.773] *** | 0.899 |
| ASP4 | $\log(TB) =$ | 3.321 [1.665 4.977] *** | + | 0.462 $\cdot \log Q$ [0.178 0.745] *** | + | 3.627 $\cdot \Delta \log Q$ [2.904 4.3503] *** | + | 0.541 $\cdot TB_{t-1}$ [0.303 0.725] *** | 0.930 |
| ASP5 | $\log(TB) =$ | 6.419 [5.496 7.341] *** | + | 0.675 $\cdot \log Q_{t+1}$ [0.523 0.827] *** | + | 0.883 $\cdot \Delta \log Q$ [0.654 1.113] *** | + | 0.405 $\cdot TB_{t-1}$ [0.279 0.531] *** | 0.865 |

TB_{t-1} showed to be significant for all subperiods except from ASP1 and ASP2. Further interpretation of the results from the multiple regression is provided in Section 8.

6.3 AUTOCORRELATION

As a last step of the regression analysis, the autocorrelation in the residuals for SSC was compared between simple linear regression relationship and relations retrieved from multiple regression analysis. To evaluate whether remaining autocorrelation was caused by the impact of previous sediment concentration, the autocorrelation was compared between multiple linear regression models including TB_{t-1} and not. If the autocorrelation in the residuals for the simple linear regression models was caused by the exclusion of important explanatory variables, the autocorrelation can be expected to have decrease for the multiple linear regression models. To evaluate the suitability of the three models, the autocorrelation was therefore compared between the three models, using the autocorrelation function (ACF) in the R program (Appendix D & G). ACF show the autocorrelation coefficients for different time lags. Autocorrelation coefficients close from 1 indicates strong autocorrelation whereas coefficients close from zero indicates little or no autocorrelation. The linear relationships are said to show significant autocorrelation if the coefficients are above the 95% confidence limit calculated as $\pm 2/\sqrt{n}$, where n is the amount of data included in the regression.

6.3.1 Results

The autocorrelation coefficients for different time lags are presented for each subperiod of July (Figure 26) and August (Figure 27).

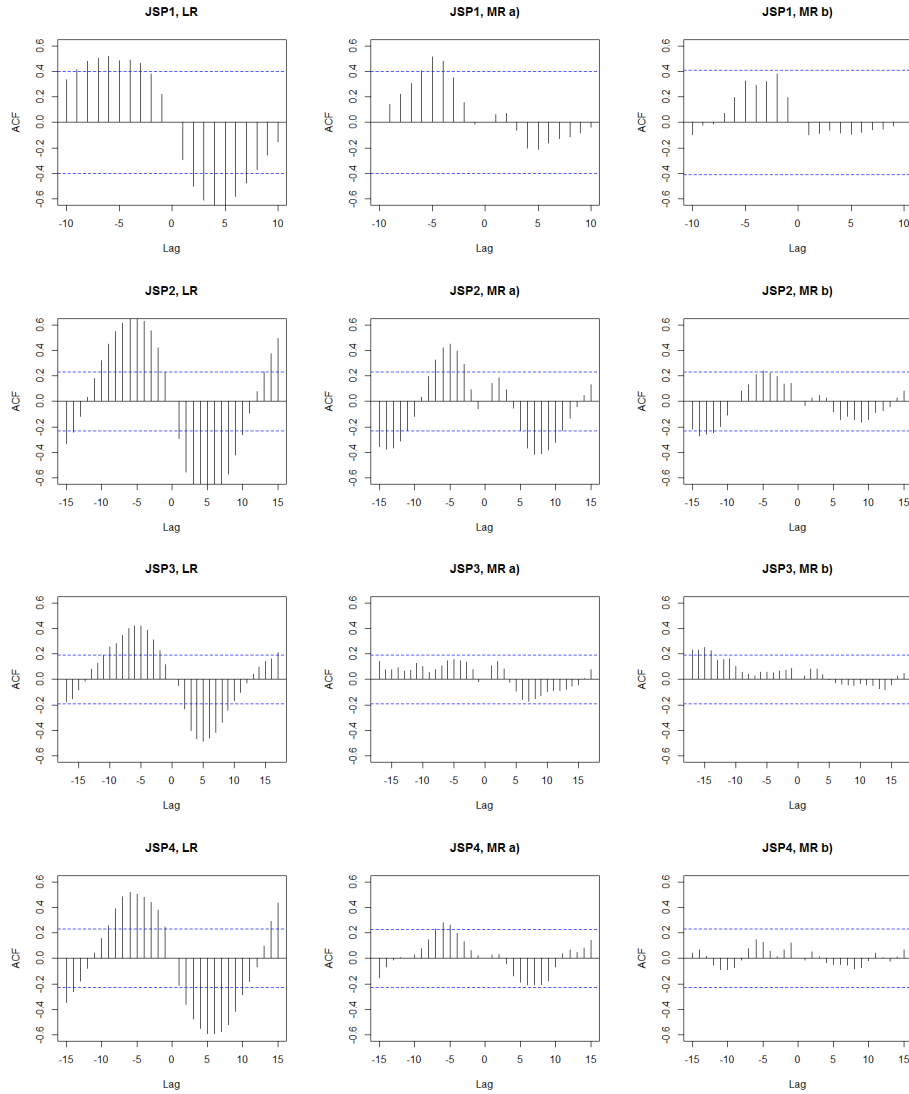


Figure 26: Autocorrelation in the residuals for SSC for subperiods in July, that is correlation between the residuals and the fitted values of SSC for different time lags. Autocorrelation for LR: simple linear regression, MR a): multiple regression analysis and MR b): multiple regression analysis including $\log(TB)_{t-1}$. Blue dotted lines represent 95% confidence interval.

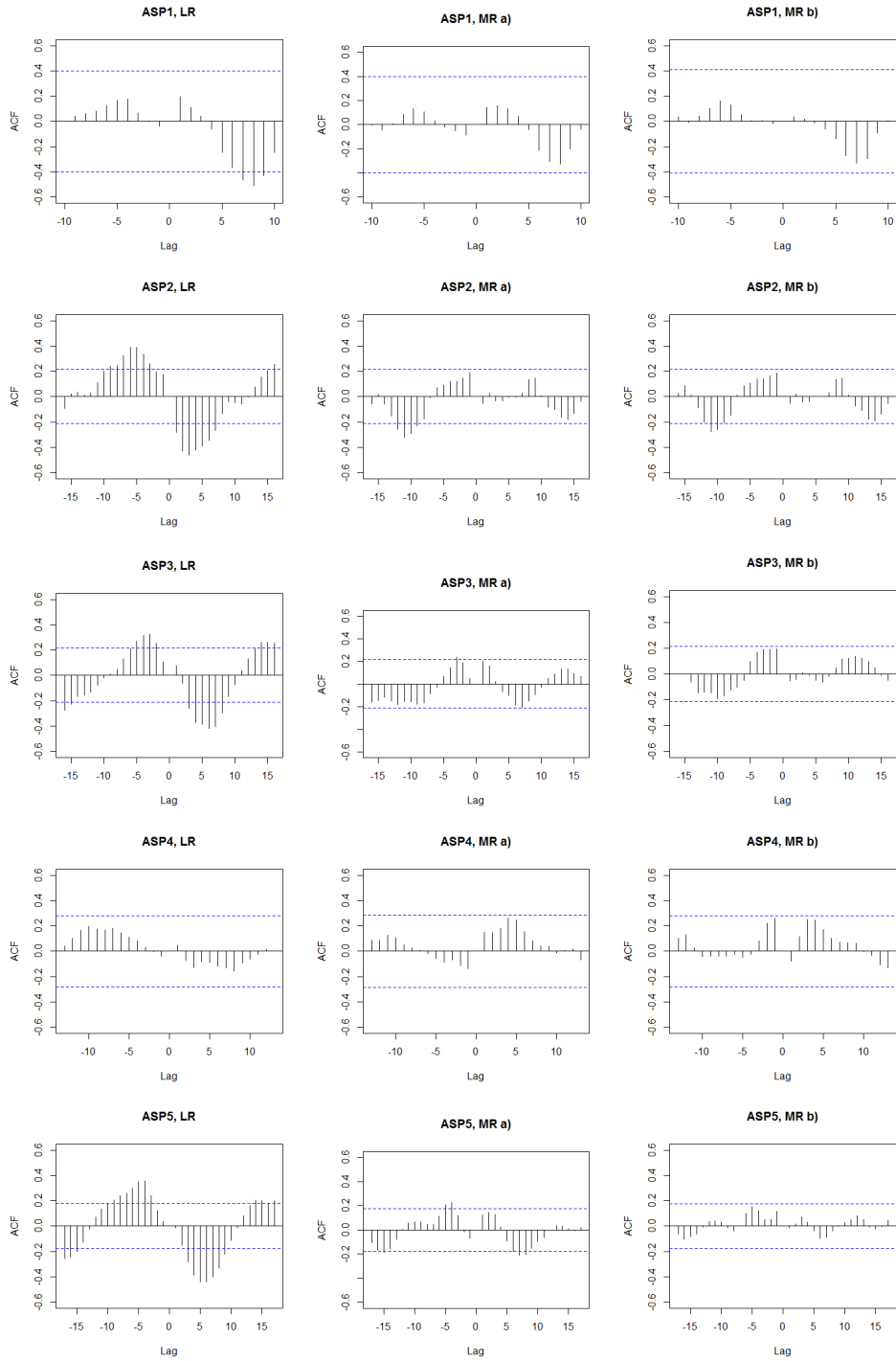


Figure 27: Autocorrelation in the residuals for SSC for subperiods in August, that is correlation between the residuals and the fitted values of SSC for different time lags. Autocorrelation for LR: simple linear regression, MR a): multiple regression analysis and MR b): multiple regression analysis including $\log(TB)_{t-1}$. Blue dotted lines represent 95% confidence interval.

In general, the autocorrelation in the SSC residuals was reduced by including other

explanatory variables than $\log Q$. In most cases, including $\log(TB)_{t-1}$ also further reduced autocorrelation. The result is further discussed in Section 8.

7 RESPONSE TO CLIMATIC VARIABLES

As the magnitude of discharge depends on melt of snow and ice as well as inputs from precipitation (Röthlisberger and Lang, 1987), changes in drainage morphology can be expected to reflect a changed response of discharge to the local meteorology. The correlation to global radiation, air temperature and precipitation for each subperiod was investigated in R, where the the cross correlation function was used to find the time delay (lag) that gave the highest correlation between two variables. In order to determine whether a possible change in lag depended on a change in time lag between global radiation and air temperature or solely on a change in the drainage systems morphology, the time lag between global radiation and air temperature was also investigated.

7.1 RESULTS

The time lag between the meteorological parameters global radiation and air temperature as well as between Q and global radiation, air temperature and precipitation are presented for July and August as well as for each subperiod respectively (Table 6).

Table 6: Time lag giving the strongest correlation between the input and the output parameter. The lag, k, is given in hours with strongest correlation for the input variable at time t+k and the output variable at time t, followed by the correlation coefficient.

| Period | n | Lag in hours (correlation) | | | |
|---------------|-----|----------------------------|------------------|-----------------|---------------|
| Input | | Global radiation | Global radiation | Air temperature | Precipitation |
| Output | | Air temperature | LogQ | LogQ | LogQ |
| July | 202 | 2 (0.531) | 3 (0.662) | 2 (0.509) | 2 (0.150) |
| JSP1 | 24 | 0 (0.852) | 2 (0.628) | 0 (0.838) | -5 (0.118) |
| JSP2 | 72 | 1 (0.793) | 3 (0.565) | 1 (0.771) | -2 (0.201) |
| JSP3 | 106 | 1 (0.642) | 3 (0.685) | 1 (0.351) | 2 (0.210) |
| JSP4 | 74 | 1 (0.880) | 3 (0.716) | 2 (0.776) | -4 (0.254) |
| August | 360 | 2 (0.453) | 3 (0.699) | 2 (0.670) | -5 (0.144) |
| ASP1 | 24 | 1 (0.724) | 3 (0.687) | 2 (0.953) | -5 (0.266) |
| ASP2 | 84 | 2 (0.729) | 3 (0.565) | 2 (0.557) | 2 (0.207) |
| ASP3 | 84 | 3 (0.600) | 4 (0.757) | 1 (0.764) | |
| ASP4 | 48 | 1 (0.857) | 2 (0.756) | 2 (0.659) | -5 (0.291) |
| ASP5 | 120 | 2 (0.543) | 3 (0.732) | 1 (0.780) | -8 (0.127) |

No clear differences could be found for the time lag between the subperiods early and late in the melting season (Table 6). The result will be further discussion in section 8.

8 DISCUSSION

Glaciers are complex and dynamic systems. This discussion therefore includes a fair amount of speculation and hypothesis of the generated results. It has to also be noted that the discussion is based on measurements and observations done at one overdeepened glaciers during one ablation season only, thus leaving ample doubt about the generalizability of the findings. Nevertheless, the discussion is considered to provide interesting information on how drainage mechanisms in overdeepened areas could work.

Some assumptions are made in this discussion, to simplify the complex nature of a glaciers drainage system: 1) clear water emerging from the glacier is assumed to have traveled through englacial or efficient subglacial channels without long contact with the bed; 2) turbid water is assumed to have traveled subglacially, in contact with the bed, i.e. probably through the slow part of the subglacial drainage system and thus through the overdeepening. These assumptions seem reasonable but are still simplifications of the reality as they do not tell how long the water has traveled along the bed and at what part of the bed. Turbid water emerging in one of the proglacial streams could for example have followed a subglacial route high up on the glacier, and later an englacial channel passing over the overdeepening. Furthermore, the hypothesis made based on results from linear regression and multiple regression analysis concern only the catchment area draining in Stream 1, thus might not be representative for the whole overdeepened area at Griesgletscher.

8.1 GRIESGLETSCHER'S SUBGLACIAL DRAINAGE SYSTEM

Tracer experiments and field observations provide, together with the bedrock topography of Griesgletscher, a picture of the morphological characteristics of the drainage system. Figure 17 reveals a main overdeepening containing various cavities. The catchment area for Stream 1 can be identified to cover only a small area located at the last part of the adverse slope. Figure 17 suggests that a bedrock ridge perpendicular to the direction of flow of ice and water, a riegel, is situated not far upglacier from Moulin A. Upglacier of this riegel, water is likely to flow down into the overdeepening and downglacier of the riegel, water will travel up the adverse slope towards Stream 1. However, important to remember is that water, except from the gravitational potential, also is affected by the overburden pressure of the ice, which might force subglacial water to flow upwards along the adverse slope and emerge in Stream 1. The discharge from Greisgletscher converges into three main streams, where Stream 1 is identified to drain a small catchment area covering a part of the adverse slope. Between the two other streams, Stream 3 had a small discharge compared to Stream 2 and it is likely that the main part of the overdeepened area is drained via a main channel on the right side of the glacier reaching Stream 2. This would mean that the water in Stream 1 does not originate from the main overdeepening. However, as the catchment area for Stream 1 seems to be located on an adverse slope, measurements done in Stream 1 are still considered to provide interesting information about subglacial drainage in overdeepened areas.

Stream 2 is carrying the biggest part of the runoff from Griesgletscher and results suggest that most of the discharge from the overdeepened area is evacuated through

a submarginal, or lateral, main channel passing on the right side of the overdeepening and emerging in Stream 2. Two factors arguing for this cause is 1) the travel time of the dye and 2) the clear colour of the water at low discharge. A glacier is typically thinner at the margins than in the middle. This makes it more efficient for water to flow along the glacier margins. The pressure in the ice depends on the shape of the bedrock as well as the ice surface and thickness and controls in which direction water will flow, as it flows towards areas of lower pressure (Shreve, 1972). The shape of the ice together with bedrock topography at Griesgletscher affects the water so that it migrates to the right side of the glacier which explains why a channel has developed here.

Even if a glacier is relatively impermeable, with discrete sets of preferential flow paths, it has a hydraulic grade line. Under this grade line, channels, pores and cavities in the ice are filled with water and above the ice is unsaturated, i.e. only partly water filled. Overdeepened areas have a permanent minimum hydraulic grade line in level with the lip of the overdeepening (Figure 28). It is common that a glacier has one or a few main channels that efficiently can evacuate the biggest part of the discharge (Röthlisberger and Lang, 1987). Water moving through a glacier carries heat that can melt ice and create channels. For this reason, channels are likely to, at one point, be located at the hydraulic grade line. This, as a channel above the hydraulic grade line will be water filled when discharge is high, but as discharge decreases at night, the channel will be only partly filled with water. Thus, more melt will occur at the bottom of the channel than at the top and the channel will wander down in the ice until it reaches the hydraulic grade line. Under this limit, the channel will at all times be water filled. Thus, as much melt will occur at the bottom as well as at the top of the channel. However, if such a main channel at Griesgletscher is already situated under the hydraulic grade line or not is unknown.

When the magnitude of Q varies over the day, the hydraulic pressure within the ice will alter as well, so that the minimum hydraulic grade line, in level with the lip of the overdeepening, raises as Q increase because of the the glacier above the overdeepening. For small Q , the main channel seems to be sufficient to evacuate all the melt water and the pressure gradient stays in level with the lip of the overdeepening. However, when Q increases during the day, the channel might not have enough capacity to evacuate all the water and water will have to find alternative routs, raising the hydraulic grade line. This causes increased pressure at the ice below and a gradient that might force subglacial water up along the adverse slope and out from the overdeepening (Figure 28). After the flood event that occurred around 1st of August, a daily change in sediment content could be seen in Stream 2. This could be explained according to previous argument, suggesting that for small Q , water was evacuated through a lateral channel, passing on the side of the overdeepening and emerging in Stream 2, showing a small flow and clear water. During the day, as melt increases, the hydraulic pressure within the ice rises and pushes water out from the overdeepening. The subglacial water originating from the overdeepening has typically a high content of suspended sediments, which could be seen in Stream 2 as the colour shifted (Figure 16). Times of clear water corresponded to times of low hydraulic pressure and water with high content of sediment is explained by water draining from the overdeepening because of high overburden pressure.

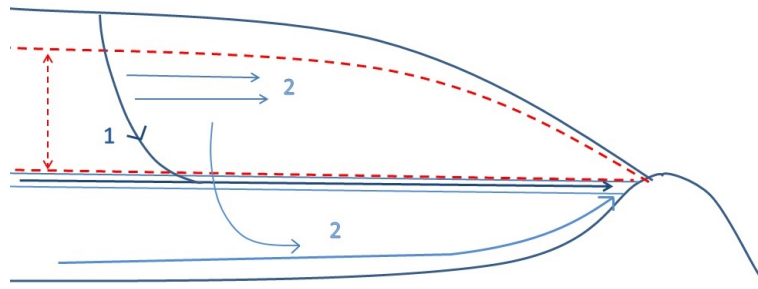


Figure 28: Sketch over drainage in the overdeepened area of Griesgletscher. The lower red line indicates a permanent hydraulic grade line and the higher line represents a raised hydraulic grade line during high discharge. 1) Indicates drainage from a moulin into an englacial or lateral channel when the hydraulic gradeline is low. 2) When the channel is no longer enough, the hydraulic grade line rises forcing subglacial water up the adverse slope.

A difference in colour between Stream 1 and Stream 2 could be seen also for high discharges when the sediment content in Stream 2 was high, suggesting different origin. When salt dilution experiments were conducted, higher background concentrations of conductivity were observed in Stream 2 than in Stream 1, further suggesting that the two streams have different main catchment areas and indicates that the residence time at the bed for the subglacial water draining in Stream 2, during high discharges, was longer than for the subglacial water emerging in Stream 1.

Linear regression for subperiods, with $\log SSC$ as dependent variable of $\log Q$, explained a high portion of the variance of SSC, indicating that Q is the most crucial variable controlling SSC. During multiple regression analysis, $\log Q$ remained one of the significant explanatory variables for all subperiods. Multiple regression analysis also revealed other explanatory variables with significant importance for SSC. Rate of change of discharge showed to be significant for every subperiod except from ASP1. This suggests that there is a difference in sediment availability for increasing and decreasing Q . Provision of sediments carried with precipitation from the sides of the valley was significant for most subperiods when precipitation occurred. Furthermore, the previous concentration of suspended sediment showed to be of importance for the current concentration and including this variable did in general reduce autocorrelation in the residuals for SSC.

To sum up, the subglacial drainage system at Griesgletscher seems to consist of one main channel, that is probably passing at the right side of the overdeepening and emerging in Stream 2. For small Q , this channel is enough to drain the main part of the glacier, but as Q increases water pressure within the ice rises and forces subglacial water out from the overdeepening. Results further suggests that a small part of the adverse slope is drained in Stream 1. Runoff on the left side of the glacier tongue, for which it is more efficient to flow towards the left, appears to be drained through Stream 3. SSC is mainly controlled by $\log Q$, the rate of change of discharge, precipitation and previous concentration of suspended sediments. Finally, these speculations strengthen the hypothesis that at Griesgletscher, the subglacial

drainage through the overdeepening is limited and that meltwater chooses a lateral rout around the overdeepening when available. This agrees with earlier observations from Storglaciären in Sweden, where tracer experiments suggested that most of the runoff traversed the overdeepening through englacial or lateral channels (Hooke and Pohjola, 1994).

8.2 SEASONAL EVOLUTION OF THE SUBGLACIAL DRAINAGE SYSTEM

In previous studies, linear regression coefficients have been used to describe the characteristics of the drainage morphology, where the gradient of the regression line represents the drainage systems capacity to evacuate sediments and the intercept indicates the relative availability of suspended sediments (Swift et al., 2005). Furthermore, changes of these coefficients propose changes of drainage system morphology (Swift et al., 2005). The two main types of drainage systems that has been described, slow and fast, have different properties and influence on sediment evacuation. In an efficient channelized drainage system, water will be evacuated through a few channels covering a small area of the bed. In such a system, exhaustion of sediments can be expected, as sediments will be flushed out by previous discharge and not replaced by new sediments (Willis et al., 1996; Hodson and Ferguson, 1999). A distributed system, on the other hand, covers a bigger area of the bed and the availability of sediments can therefore be expected to be higher with a more constant concentration. In this study, Q and SSC were monitored only in Stream 1. Thus, regression analysis reflects only a small part of Griesgletscher's subglacial drainage system.

Investigation of the linear regression relationships (Table 3, Figure 5) reveal subperiods that stands out. ASP3 presents lower gradients than all other subperiods and JSP4 show a significantly lower gradient than JSP3 and ASP4, thus indicating that the drainage systems was less efficient in evacuating sediments during these periods. JSP4 shows the widest range of Q, including the lowest minimum Q. However, considering only high Q, same Q during JSP4 or ASP3 would have less capacity to evacuate sediments than during remaining subperiods. It is the velocity of the water that determines how capable it is to lift and entrain sediments. Water flowing with a high velocity have more energy to lift and entrain sediments. This suggests that water was travelling through the drainage system with smaller velocities during these periods compared to the remaining. An explanation for this could be that the melt production was slower at this time. During days of high melt, the difference in Q between day and night is big and a typical hydrograph would show a peaked curve with a steep rising limb. At days with low Q, the daily peak is lower and the hydrograph typically presents a less peaked curve with a flatter rising limb. If the drainage system is resembled with a pipe of fixed size, the velocity of water travelling through this pipe would depend on the gradient of the hydrographs rising limb. If the rise is fast, a lot of water suddenly wants to travel through the pipe, causing high velocities. Thus, these two periods could potentially be periods with a smaller gradient of the rising limb, causing smaller velocities. However, analysis of the gradient of the rising limb of the hydrographs for different subperiods does not reveal any differences.

Another explanation for the behaviour during JSP4 and ASP3 could be the presence of a temporary obstacle in the drainage system, causing lower velocities. Drainage paths could be affected by glacier movement or blocking by sediments. After that new drainage routes are established, the capacity to evacuate sediments would as well reestablish to previous levels. If the meltwater is forced to find alternative routes, new areas of the bed would be reached. Thus, the availability of suspended sediments could be expected to increase as soon as new routes are defined. Results indicate that the availability of suspended sediment was lower during ASP3, but increased again during ASP4. Records of EC could provide additional information regarding seasonal or short term changes in drainage morphology. An increase in EC coincides with the ending of ASP3. After this event, the conductivity remained relatively constant until the end of August, but at a higher level than before. This could possibly be explained by an interruption of drainage paths during ASP3 and establishment of new routes. If it was the first time that meltwater flowed through these new paths, this would be expected to cause an increase in EC. This, as a high concentration of ions could be expected at these areas of the bed, as a result of a long retention time before this event.

In general, EC was high in the beginning of the season and noteworthy lower in August. Cloudy or cold weather seem to be followed by temporary higher values of conductivity. The same result was reported at Haut Glacier d'Arolla, where EC decreased as Q increased in the beginning of the ablation season. Later in the season, higher values of EC followed after weather generating lower runoff (Swift et al., 2002). In general, high EC in the beginning of the ablation season can be explained by that part of the water draining subglacially at this time could have been stored subglacially since the last summer. Thus, with such a long residence time, higher conductivity could be expected (Fenn, 1987). At Griesgletscher, the conductivity remained high until the flood event. It is likely that water that had been stored in the glacier was flushed out at this time, resulting in lower conductivity in August.

Results from linear regression analysis also indicate that the capacity to evacuate sediments was significantly higher during JSP1 than for the rest of the periods. Furthermore, JSP1 shows a significantly higher intercept than all other subperiods except from ASP1. JSP1 represents the first 24 hours of the field campaign and due to the lack of knowledge of the behaviour of the SSC- Q relation before this subperiod, it is hard to draw any conclusions about the extension of these results.

In conclusion, the results from the linear regression analysis suggest that there are no clear seasonal differences in morphology for the drainage systems on the adverse slope forming the catchment area of Stream 1. This conclusion is strengthened from the investigation of time lags to climatic variables, which neither reveal any seasonal differences. Consequently, this confirms the hypothesis that the evolution of the subglacial drainage system feeding Stream 1 is highly restricted. This further agrees with studies made at Storglaciären, where high basal water pressures were observed in the overdeepened area throughout the ablation season, indicating inefficient drainage (Jansson, 1995). However, the results from the linear regression analysis are not representative for the whole overdeepened area of Griesgletscher,

but concerns only the catchment area of Stream 1. Moreover, results from salt dilution experiments indicate that Stream 1 only contains a small portion of subglacial water (Figure 19). It is therefore likely that the calculated time lags are more representative for the supraglacial part of Stream 1 than the subglacial part and might explain the absence of seasonal evolution in time lag.

Even though no seasonal evolution of the drainage system seems to take place, the result indicates that the relationship between SSC and Q is sensitive to temporary changes. Regarding the subglacial drainage system in total, dye tracing experiments performed in Moulin C indicates that the drainage path from Moulin C to Stream 2 got more efficient throughout the season. This, as the travel time was shorter in August than in July. However, the only injection that gave detection from Moulin C in August was made in the morning just before that subglacial water started to drain in Stream 2. If previous hypothesis are true, this would be the time of the day that the drainage from Moulin C was most efficient, i.e. the highest Q before that subglacial water drains. Previous studies based on tracer experiments suggests that the travel time from a moulin depends both on the magnitude of the discharge and the water level in the moulin (Werder et al., 2010). Werder et al. (2010) performed frequent dye injections during 24 hours. At the same time, Q of the meltwater entering the moulin was monitored. They concluded that for high Q , the time for the dye to travel through the moulin would be longer, because of the high water level in the moulin. At the same time, high Q would mean a faster velocity through englacial channels. Similarly, the water level in the moulin would decrease for low Q , allowing the dye to travel faster through the moulin. However, at this time the velocity through englacial channels would be lower (Werder et al., 2010)

8.3 COMPARISON TO NON-OVERDEEPEINED GLACIERS

Finally, does the morphological characteristics and seasonal evolution of Griesgletscher's subglacial drainage system differ from a non-overdeepened glacier? This study suggests that the subglacial drainage system for the overdeepened area at Griesgletscher that emerges in Stream 1, stayed distributed throughout the ablation season 2017. Consequently, the evolution from an inefficient and distributed system to an efficient channelized system that has typically been observed for non-overdeepened glaciers did not take place. Comparing the coefficients from the linear regressions made between SSC and Q measurements at Griesgletscher to similarly made linear regression models at non-overdeepened Haut Glacier d'Arolla, performed by Swift et al. (2005), coefficients for $\log Q$ at Griesgletscher are lower. That is true also for coefficients for $\log Q$ obtained at Haut Glacier d'Arolla from early season subperiods, represented by distributed, inefficient drainage. These coefficients were at Haut Glacier d'Arolla between 1.283 - 1.355 compared to 0.531 - 0.931 during the whole ablation season at Griesgletscher, except from JSP1 for which the coefficient for $\log Q$ was 1.610. This indicates that the efficiency to evacuate suspended sediments at Griesgletscher was lower than the efficiency observed in the beginning of the ablation season at Haut Glacier d'Arolla. At Haut Glacier d'Arolla, a sudden rise of the gradient for the linear relationships between SSC and Q was observed from the middle of July and relationships between SSC and Q for the following subperiods showed similarly high gradients, 2.152 - 2.857, until the

end of the monitoring program in middle of August (Swift et al., 2005). Furthermore, a decrease of sediment availability was seen from the beginning of the season, when sediment availability was high, but the capacity to evacuate suspended sediments low. In the end of the season, the sediment availability had increased despite sediment exhaustion and the capacity to evacuate suspended sediments was higher (Swift et al., 2005). Swift et al. (2005) suggested that the increased availability of suspended sediments was due to an additional sediment delivery mechanism to channels in the late summer (Hubbard et al., 1995).

Multiple regression analysis conducted by Swift et al. (2005), from measurements made at Haut Glacier d’Arolla, suggests that the significant explanatory variables for $\log SSC$ were $\log Q$, rate of change of discharge, days since discharge was equaled or exceeded and precipitation. In this study, similarly, $\log Q$, rate of change of discharge and precipitation were significant explanatory variables, but days since discharge was equaled or exceeded was significant only for ASP3. This variable represents the alteration of sediment availability caused by sediment exhaustion due to previous discharges. Such sediment exhaustion can be expected for a channelized system, but not for a distributed system. ASP3 is one of the subperiods for which a relocation of drainage routes might have taken place, which could explain the importance of this variable during this period.

The study at Haut Glacier d’Arolla further suggests that the sediment concentration at time t was highly dependent on the concentration at time $t-1$. The same phenomenon was seen at Griesgletscher for most subperiods, where introduction of SSC_{t-1} reduced autocorrelation in the residuals. This variable could be expected to be important in any kind of drainage system, as it mainly points out that velocities for which suspended sediments are deposited from the water is lower than the velocity for when sediments are entrained.

In conclusion, the results obtained in this thesis points in the direction that the morphology of the drainage system that covers the catchment area for Stream 1, as well as the sediment evacuation mechanisms and seasonal evolution are different from what has earlier been observed at non-overdeepened glaciers. However, results also suggests that the area addressed only represents a small part of Griesgletscher’s drainage system. Thus, further investigation of the evacuation of suspended sediments in the three proglacial streams is needed to fully characterize the morphology of the subglacial drainage system at Griesgletscher.

8.4 PRACTICAL CONSIDERATIONS AND ENCOUNTERED PROBLEMS

This report is based on results from fieldwork performed during the ablation season 2017. Conducting measurements in a turbid stream is not performed without problems. The most frequent problem was the sensors getting clogged by sediments or filled with rocks. One difficult but important aspect was therefore the placement of the sensors. If put too low, the turbidity sensors will monitor the amount of sediments at the bottom, instead of the turbidity caused by suspended sediments that was of interest. Furthermore, putting the sensors too high would result in the sensors being positioned above the water surface at low discharges. At the same time, the possibility to choose different positions for the sensors was limited because

of the low water level in Stream 1. The position of the sensors was evaluated and sometimes adjusted at visits of the gauging station and the sensors cleaned if needed. To ensure the collection of turbidity measurements, two turbidity sensors were used. During analysis of the data, periods for which the sensors were clogged or above the surface could be identified as the measurement would show a constant value instead of fluctuations captured by the other sensor. If different trends were seen between the two sensors, the data was further evaluated to make sure that accurate values were used for analysis. When one sensor was clogged, the values from the other sensor could be used. A mean of the two turbidity sensors have been used at times at which they were both working as they should. Another point affecting the results was that the range of the turbidity meters (1800) was sometimes exceeded, meaning that the measurements will miss the true maximum values of the turbidity. However, the time that the turbidity exceeded the maximum values was very short, why this was considered to not affect the result drastically.

The same problem of positioning applies for the inlet of the automatic water sampler. If a part of the inlet is situated above the water surface, no water sample will be collected. If, however, the inlet is put too close from the bed of the stream, the water sample will not only contain suspended sediments, but also bigger sediments from the bottom. The fact that Stream 1 was not very deep, made the choice for placement very limited, and missing out of some water samples was considered better than putting the inlet closer from the bottom. Another problem with the automatic water sampler is that it takes a point sample, representing the whole cross section area. However, as the water in Stream 1 was turbid, the mixing was high and helped to make the SSC more evenly distributed over the cross section (Gurnell, 1987).

The result from the calibration between TB and SSC showed a poor fit and scattered data points (Figure 11). One explanation for this could be that the placement of the inlet not was ideal. Another explanation could be that the volume of the samples was too small to give an accurate concentration of suspended sediments. As the content of sediments was high, the volume was reduced to 350 ml. This because filtering of big volumes of water with a lot of sediments through a filter paper is very time consuming. A weight of at least 0.1 g of sediments was considered to be required to give an accurate weight and for this 350 ml was enough. However, in retrospect it can be noted that the small volume might have caused the scatterness of the data points for the TB – SSC relationship. No clear pattern in the distribution between water samples collected before and after the reinstallation of the gauging station could be seen, why the same calibration was considered as representative for the whole period. The automatic water sampler was programmed to collect water samples that would cover the whole range of discharges, it was however mostly for low water levels that water samples were missing. This was compensated by a 24 hour measuring campaign when water samples were collected manually every hour. Water samples collected manually were less scattered (Figure 11). There is also a portion of uncertainty from the handling of the water samples during the filtering process and sediments can have been lost when changing bottle of the water sample etc. Effort was therefore put into minimizing the loss of sediments in the different steps.

For the conductivity meter and the pressure transducer, sediment also caused prob-

lems by clogging the sensors. Unfortunately there is a big data gap when the pressure transducer was not working because it got filled with sediments. This will in a future study be filled by modeling of Q and might reveal further information about the SSC- Q relation.

The turbid water also caused problems when measuring fluorescence during tracer experiments, as the turbidity affects the readings. Sedimentation caused increasing readings after that the water samples had been injected in the fluorometer. Obtaining stable readings was therefore problematic. The approach of letting samples rest before injection in the fluorometer and noting three values after 15, 30 and 60 seconds respectively facilitated the measurements and resulted in more stable readings. Last, measuring of discrete water samples might have resulted in that the detection, or the peak of the detection, was missed.

At last, when performing salt dilution experiments, it was problematic to find suitable locations for injection and monitoring of the conductivity. The distance between the injection and the measuring point has to be long enough for the salt to mix well in the water, but if the sensors were placed where the water moved too wildly, they got flushed around and could end up above the surface.

9 CONCLUSION

Summarized below are conclusions made based on field data collected at Griesgletscher during the summer 2017. However, these conclusions are speculative. Monitoring of the three proglacial streams emerging from Griesgletscher, during more than one ablation season is required in order to 1) make more credible conclusions and 2) make conclusion that are representative for the whole subglacial drainage system at Griesgletscher. Furthermore, in order to establish whether the behavior of the subglacial drainage system that has been observed at Griesgletscher reflects the typical behavior of subglacial drainage at overdeepened glaciers, similar studies at other overdeepened glaciers are compulsory.

The answers to the research questions are as follows:

- The overdeepened area of Griesgletscher is drained mainly via a lateral channel running along the orographic right glacier margin. Subglacial water from the overdeepening is drained mainly when discharge is high and when subglacial water is forced out of the overdeepening because of a rise in water pressure. The evacuation of suspended sediments is predominated by discharge, but depends also the rate of change of discharge, precipitation and previous concentration of suspended sediments.
- The morphology of the subglacial drainage system on the adverse slope draining in Stream 1 is likely to be distributed or consisting of a network of channels. No seasonal increase in efficiency to evacuate suspended sediments was found for this area.
- The evolution of the subglacial drainage systems morphology typical for a non-overdeepened glaciers could not be seen for the catchment area of Stream 1. This area seems to be located on an adverse slope, suggesting that the evolution of a more efficient drainage system on the adverse slopes is restricted.

10 REFERENCES

- Alley, R., Cuffey, K., Evenson, E., Strasser, J., Lawson, D., and Larson, G. (1997). How glaciers entrain and transport basal sediment: Physical constraints. *Quaternary Science Reviews*, 16(9):1017–1038.
- Alley, R. B., Lawson, D. E., Evenson, E. B., Strasser, J. C., and Larson, G. J. (1998). Glaciohydraulic supercooling: a freeze-on mechanism to create stratified, debris-rich basal ice: II. theory. *Journal of Glaciology*, 44(148):563–569.
- Anderson, S. P., Fernald, K. M., Anderson, R. S., and Humphrey, N. F. (1999). Physical and chemical characterization of a spring flood event, bench glacier, Alaska, U.S.A.: evidence for water storage. *Journal of Glaciology*, 45(150):177–189.
- Beecroft, I. (1983). Sediment transport during an outburst from Glacier de Tsidjiore Nouve, Switzerland, 16–19 june 1981. *Journal of Glaciology*, 29(101):185–190.
- Bezinge, A. (1987). Glacial meltwater streams, hydrology and sediment transport: The case of the grande dixence hydroelectricity scheme. In *Glacio-Fluvial Sediment Transfer*, volume 1, pages 473–498. John Wiley & Sons, New York.
- Cook, S. J. and Swift, D. A. (2012). Subglacial basins: Their origin and importance in glacial systems and landscapes. *Earth-Science Reviews*, 115(4):332–372.
- Creyts, T. T. and Clarke, G. K. C. (2010). Hydraulics of subglacial supercooling: Theory and simulations for clear water flows. *Journal of Geophysical Research*, 115(F3):F03021.
- Feiger, N., Huss, M., Leinss, S., Sold, L., and Farinotti, D. (2018). The bedrock topography of gries- and findelengletscher. *Geographica Helvetica*, 73(1):1–9.
- Fenn, C. (1987). Electrical conductivity. In *Glacio-Fluvial Sediment Transfer*, volume 1, pages 377–414. John Wiley & Sons, New York.
- Fountain, A. G. (1992). Subglacial water flow inferred from stream measurements at South Cascade Glacier, Washington, U.S.A. *Journal of Glaciology*, 38(128):51–64.
- Fountain, A. G. and Walder, J. S. (1998). Water flow through temperate glaciers. *Reviews of Geophysics*, 36(3):299–328.
- Gomez, B. (1987). Bedload. In *Glacio-Fluvial Sediment Transfer*, volume 1, pages 355–376. John Wiley & Sons, New York.
- Gurnell, A. (1987). Suspended sediment. In *Glacio-Fluvial Sediment Transfer*, volume 1, pages 305–354. John Wiley & Sons, New York.
- Gurnell, A. M. (1982). The dynamics of suspended sediment concentration in an alpine pro-glacial stream network. *Hydrological Aspects of Alpine and High Mountain Areas*, pages 319–330.
- Helsel, D. R. and Hirsch, R. M. (1993). *Statistical Methods in Water Resources*, volume 49. Elsevier, New York.

- Hock, R. and Hooke, R. L. (1993). Evolution of the internal drainage system in the lower part of the ablation area of Storglaciären, Sweden. *Geological Society of America Bulletin*, 105(4):537–546.
- Hodgkins, R. (1999). Controls on suspended-sediment transfer at a high-arctic glacier, determined from statistical modelling. *Earth Surface Processes and Landforms*, 24(1):1–21.
- Hodson, A. J. and Ferguson, R. I. (1999). Fluvial suspended sediment transport from cold and warm-based glaciers in svalbard. *Earth Surface Processes and Landforms*, 24(11):957–974.
- Hooke, R. L. (1991). Positive feedbacks associated with erosion of glacial cirques and overdeepenings. *Geological Society of America Bulletin*, 103(8):1104–1108.
- Hooke, R. L. and Pohjola, V. A. (1994). Hydrology of a segment of a glacier situated in an overdeepening, Storglaciären, Sweden. *Journal of Glaciology*, 40(134):140–148.
- Hubbard, B. P., Sharp, M. J., Willis, I. C., Nielsen, M. K., and Smart, C. C. (1995). Borehole water-level variations and the structure of the subglacial hydrological system of Haut Glacier d’Arolla, Valais, Switzerland. *Journal of Glaciology*, 41(139):572–583.
- Iken, A., Röthlisberger, H., Flotron, A., and Haeberli, W. (1983). The uplift of Unteraargletscher at the beginning of the melt season—a consequence of water storage at the bed? *Journal of Glaciology*, 29(101):28–47.
- Jansson, P. (1995). Water pressure and basal sliding on Storglaciären, northern Sweden. *Journal of Glaciology*, 41(138):232–240.
- Lawson, D. (1995). Sedimentary and hydrologic processes within modern terrestrial valley glaciers. In *Modern glacial environments: processes, dynamics and sediments*, volume 1, pages 337–363. Butterworth-Heinemann, Oxford.
- Nienow, P. W., Sharp, M., and Willis, I. C. (1998). Seasonal changes in the morphology of the subglacial drainage system, Haut Glacier d’Arolla, Switzerland. *Earth Surface Processes and Landforms*, 23:825–843.
- Nye, J. F. and Frank, F. C. (1973). Hydrology of the intergranular veins in a temperate glacier. In *Symposium on the Hydrology of Glaciers*, pages 157–161. Proceedings of the symposium held at Cambridge, England, 7–13 September 1969, IAHS Publication No. 95.
- Raymond, C., Benedict, R., Harrison, W., Echelmeyer, K. A., and Sturm, M. (1995). Hydrological discharges and motion of fels and black rapids glaciers, Alaska, U.S.A.: implications for the structure of their drainage systems. *Journal of Glaciology*, 41(138):290–304.
- Raymond, C. F. (1987). How do glaciers surge? a review. *Journal of Geophysical Research: Solid Earth*, 92(B9):9121–9134.

- Röthlisberger, H. (1968). Erosive processes which are likely to accentuate or reduce the bottom relief of valley glaciers. In *General assembly of Bern (25 sept. - 7. oct. 1967)*, pages 87–97. IAHS. Publication No. 79.
- Röthlisberger, H. (1972). Water pressure in intra- and subglacial channels. *Journal of Glaciology*, 11(62):177–203.
- Röthlisberger, H. and Lang, H. (1987). Glacial hydrology. In *Glacio-Fluvial Sediment Transfer*, volume 1, pages 207–303. John Wiley & Sons, New York.
- Shreve, R. L. (1972). Movement of water in glaciers. *Journal of Glaciology*, 11(62):205–214.
- Souchez, R. and Lorrain, R. (1987). The subglacial sediment system. In *Glacio-Fluvial Sediment Transfer*, volume 1, pages 147–164. John Wiley & Sons, New York.
- Swift, D. A., Nienow, P. W., and Hoey, T. B. (2005). Basal sediment evacuation by subglacial meltwater: suspended sediment transport from Haut Glacier d’Arolla, Switzerland. *Earth Surface Processes and Landforms*, 30(7):867–883.
- Swift, D. A., Nienow, P. W., Spedding, N., and Hoey, T. B. (2002). Geomorphic implications of subglacial drainage configuration: rates of basal sediment evacuation controlled by seasonal drainage system evolution. *Sedimentary Geology*, 149(1-3):5–19.
- Tangborn, W. V., Krimmel, R. M., and Meier, M. F. (1975). A comparison of glacier mass balance by glaciological, hydrological and mapping methods, south cascade glacier, Washington. *International Association of Hydrological Sciences Publication*, 104:185–196.
- Werder, M. A., Schuler, T. V., and Funk, M. (2010). Short term variations of tracer transit speed on alpine glaciers. *The Cryosphere*, 4:381–396.
- Willis, I. C. (1995). Intra-annual variations in glacier motion: a review. *Progress in Physical Geography*, 19(1):61–106.
- Willis, I. C., Richards, K. S., and Sharp, M. J. (1996). Links between proglacial stream suspended sediment dynamics, glacier hydrology and glacier motion at Midtdalsbreen, Norway. *Hydrological Processes*, 10(4):629–648.

APPENDIX A. Calibration of turbidity measurements

R code used for calibration of turbidity –suspended sediment concentration relation.

```
#Set working directory
setwd("C:/Users/Marie/Desktop/R")
#Load packages
library(chron)
library(ggplot)
#Accept NA
na.rm=TRUE
options(stringsAsFactors=FALSE)

#Load data
ct=read.csv("SSC_turbidity_calibration.csv")

#create a chron object, time serie combining date and time
dtsct<-(ct$Date)
tmsct<-(ct$Time)
xct <- chron(dates = dtsct, times = tmsct,
format = c(dates="d/m/y", times="h:m:s"))

#Perform linear regression between LogSSC and logTB
fit_SSC_turb<-lm(log10(ct$Turbidity)~log10(ct$SSC))
#Show summary of statistics
summary(fit_SSC_turb)

#Plot data and linear regression with 95 % CI
ggplot(ct, aes(log(Concentration..mg.L.), log(Turbidity)))
+geom_point(color="blue") + stat_smooth(method='lm')
+ xlab("log10(SSC_ [mg/l])") + ylab("log10(Turbidity)")

#Divide data into 3 parts:
# 1) Before flood event
# 2) 24 hour campaign
# 3) After flood event
a1<-ct$Concentration..mg.L.[1:49]
a2<-ct$Concentration..mg.L.[50:74]
a3<-ct$Concentration..mg.L.[75:115]
b1<-ct$Turbidity[1:49]
b2<-ct$Turbidity[50:74]
b3<-ct$Turbidity[75:115]
plot(a1, b1)

#Save as data frame
ct2<-as.data.frame(a1, a2, a3, b1, b2, b3)

#Plot data with different colors for different periods
#Plot also linear regression with 90 % CI
ggplot() +
  geom_point(data = ct2, aes(x = SSC1, y = Turb1),
```

```
color = "blue", size = 2)
+ geom_point(data = ct2, aes(x = SSC2, y = Turb2),
color="darkgreen", size = 2)
+ geom_point(data = ct2, aes(x = SSC3, y = Turb3),
color = "darkred", size = 2)
+ stat_smooth(data = ct2, aes(x = SSC, y = Turbidity),
method = "lm", color = "darkblue")
+ xlab("log(SSC[mg/l])") +ylab("log(Turbidity)")
+ scale_x_log10() + scale_y_log10()
```

APPENDIX B. Calculation of discharge

R code used to calculate hourly values for water filled cross section area of Stream 1 and to calibrate a relation between cross section area and discharge obtained from salt dilution experiments. As the cross section profile changed over the season, different cross section profiles were used for different times of the season. Here follows an example from calculation of the cross section profile from the first week of July.

```
#Set working directory
setwd("C:/Users/Marie/Desktop/R")
options(stringsAsFactors=FALSE)
#Accept NA
na.rm=TRUE
#Load packages
library(chron) #To work with time series considering time and date
library(xts) #Also loads zoo, to plot time series with date and time in ggplot
library(ggplot2) #For plotting
library(gridExtra) #To arrange plots as subplots
library(scales) #To scale x and y axes in plots
library(sf)
library(st) #To create a polygon and calculate its area

#Load hourly data for July
JH=read.csv("J_hourly.csv")
#create a chron object, time serie combining date and time
dtsJH<-(JH$Date)
tmsJH<-(JH$Time)
TimeDateJH <- chron(dates = dtsJH, times = tmsJH,
                    format = c(dates="m/d/y", times="h:m:s"))

#Load data for the cross section data.
#Create vector for the width of the cross section profile.
#The width of the cross section profile in July, x_profileJ, was 500 cm.
#For August, the width was 450 cm.
#The hight of the cross section profile was measured every 25 cm.
cross_section_dataJ<-read.csv("Cross_sec1.csv")
x_profileJ<-seq(0,500,25)
y_profileJ<-cross_section_dataJ$X2.Jul

# Create matrix with coordinates from x and y profiles
mJ <- matrix(c(0, x_profileJ, 500, 0, 0, -y_profileJ, 0, 0),
             byrow = FALSE, ncol = 2)

# Create a polygon
polyJ <- st_polygon(list(mJ))
# View the polygon
plot(polyJ)
# Calcualte the area
st_area(polyJ)
#plot the cross section with water level for example 40 cm.
plot(filler(40, polyJ, x_profile, y_profile), add=TRUE, col="green")
```

```

#Data was available as hourly means for water pressure.
#Calculate water level from water pressure [cm]
depthJ <- (0.015+(-1)*JH$Ptrans[1:202]*6.89475729/(9.81))*100

#Fill the cross section profile with water up to measured water level,
#starting from the deepest point of the cross section profile.
filler <- function(depthJ, profile, x_profileJ, y_profileJ, xdelta=100, ydelta)
  dJ= -(max(yprofJ))+depthJ
  xrJ = range(xprofJ)
  yrJ = range(-yprofJ)
  xdelta = 100
  xcJ = xrJ[c(1,2,2,1,1)] + c(-xdelta, xdelta, xdelta, -xdelta, -xdelta)
  ycJ = c(dJ, dJ, min(yrJ)-ydelta, min(yrJ)-ydelta, dJ)
  water = st_polygon(list(cbind(xcJ,ycJ)))
  st_intersection(profile, water)
}

#Calculate the water filled cross section area for various depth
areaJ<- function(depthJ)st_area(filler(depthJ, polyJ, x_profileJ, y_profileJ))
MatrixLJ <- lapply(depthJ, areaJ)
names(MatrixLJ) <- depthJ
#Save depth in table
table_csaJ <- as.data.frame(MatrixLJ)

# Save water filled cross section areas as CSV file.
write.csv(table_csaJ, file = "cross_sectionJ1.csv")

#Calibrate a relationship between water filled cross section area and Q
#Load data for Q and cross section area
Q_data=read.csv("Q_data1.csv")

#Perform linear regression between Q and cross section area
Q_A<-lm(Q_data$Q2~Q_data$m2)
#Show summary of statistics
summary(Q_A)

#Plot the relation with 95% confidence interval
ggplot(Q_data, aes(m2,m3.s))+geom_point()+ stat_smooth(method='lm')
+ xlab("Cross_section_area_[m^2]") + ylab("Discharge [m^3/s]")

#Set the intercept to 0
I_0 <- lm(Q_data$Q1~Q_data$m2+0)
#Show summary of statistics
summary(I_0)
#Create a line from the relation
QH<-Q_data$m2*I_0$coefficients

#Plot the relation
ggplot(Q_data, aes(m2,Q1))+geom_point()+ stat_smooth(method='lm')

```

APPENDIX C. Plot variables and weather data

R code for plot of measured variables and weather data (Figure 13).

```
setwd("C:/Users/Marie/Desktop/R")
#Load packages
library(chron) #To use time series with date and time
library(ggplot2) #For plotting
library(gridExtra) #To arrange plots as subplots
library(scales) #To scale x and y axis in plots
options(stringsAsFactors=FALSE)
#Accept NA
na.rm=TRUE

#Load data for hourly values
TH=read.csv("Tot_h.csv")
#Create a chron object, time serie object combining date and time
dtsTH<-(TH$Date)
tmsTH<-(TH$Time)
TimeDateTH <- chron(dates = dtsTH, times = tmsTH,
                    format = c(dates="m/d/y", times="h:m:s"))

#Calculate daily running mean for air temperature and global radiation
smoothIndexTemp2 <- rollmean(x = TH$Airtemp.2, #Original series
                             width=24, #Width of the window
                             k=24) #Time step
SmoothIndexRad <- rollmean(x = TH$Rad, #Original series
                           width=24, #Width of the window
                           k=24) #Time step

#Plot every variable over time
graph1<-ggplot(TH, aes(TimeDateTH,SSC))+geom_line()
+ scale_x_chron() +xlab("")+ylab("SSC_[g/l]")
graph2<-ggplot(TH, aes(TimeDateTH,Q))+geom_line()
+ scale_x_chron() +xlab("")+ylab("Q_[m3/s]")
grid.arrange(graph12, graph11, graph9, graph3, graph4, graph5, nrow=6)
graph3<-ggplot(TH, aes(TimeDateTH,CorrEC))+geom_line()
+ scale_x_chron()+coord_cartesian(ylim = c(0, 0.1))
+xlab("")+ylab("EC_[mS/cm]")
graph4<-ggplot(TH, aes(TimeDateTH,Prec))+geom_area()
+ scale_x_chron() +xlab("")+ylab("Precipitation_[mm]")
+expand_limits(y=c(0,10))
graph5<-ggplot(TH, aes(TimeDateTH,Rad))+geom_line(color="darkgrey")
+ geom_line(aes(TimeDateTH,SmoothIndexRad)) + scale_x_chron()
+xlab("")+ylab("Global_radiation_[W/m2]")
graph6<-ggplot(TH, aes(TimeDateTH,Airtemp.2))+geom_line(color="darkgrey")
+geom_line(aes(TimeDateTH,smoothIndexTemp2))
+scale_x_chron()+xlab("")+ylab("Air_temp._2_m_[C]")

#Arrange all variables above each other in one plot
grid.arrange( graph1, graph2,graph3,graph4,graph5,graph6, nrow=6)
```

APPENDIX D. Linear regression

R code used for linear regression for full period and for subperiods.

```
setwd("C:/Users/Marie/Desktop/R")
#Load packages
library(xts) # this also loads zoo
library(chron) #To create date-time object
library(ggplot2) #For plots
library(gridExtra) #To arrange subplots
library(scales) #To scale axes in plots
na.rm=TRUE #Accept NA

#load data wiht hourly averrages
JH2=read.csv("J_hourly_full_2_10.csv")

#create a chron object, time serie combinining date and time
dtsJH2<-(JH2$Date)
tmsJH2<-(JH2$Time)
TimeDateJH2 <- chron(dates = dtsJH2, times = tmsJH2,
format = c(dates="m/d/y", times="h:m:s"))

#Perform linear regression for July,
#save slope, intercept and residuals.
#Show summary of statistics
fit_July<-lm(log10(JH2$SSC)~log10(JH2$Q))
SlopeJ<-coefficients(fit_July)[2]
InterceptJ<-coefficients(fit_July)[1]
residuals_J<-resid(fit_July)
summary(fit_July)

#Creat daily mean of residuals
SmoothIndexResidualsJ <- rollmean(x = residuals_J, #Original series
width=24, #24 hour mean
k=24, #24 hour time step
fill = NA) #Fill head and tail with NA

#Plot residuals for July
d = data.frame(x=TimeDateJH2,y=SmoothIndexResidualsJ,z=residuals_J)
Resid_July<-ggplot(d, aes(x,y))
+ geom_area(data=subset(d, y<=0), fill="blue")
+ geom_area(data=subset(d, y>=0), fill="orange")
+ scale_x_chron() + scale_y_discrete(limits=c(-1.5,-1,-0.5,0,0.5,1,1.5))
+ geom_line(aes(x,z), color="darkgrey")
+ geom_line(aes(x,y))+xlab("")+ylab("Residual, _SSC") + ggtitle("July")

#Find time lag that give highest correlation between log(SSC) and log(Q)
a=log10(JH2$SSC)
b=log10(JH2$Q)
d <- ccf(a, b, plot = FALSE)
cor = d$acf[, ,1]
lag = d$lag[, ,1]
res = data.frame(cor, lag)
```

```

res_max = res[which.max(res$cor),]
print(res_max)

#Perform linear regression for subperiods,
#save slopes, intercept and residuals.
#Show summary of regression.
#Create autocorrelation diagram for residuals and fitted values.

#Regression JSP1, 1 h lag for Q.
RegJ_1<-lm(log10(JH2$SSC[1:24])~log10(JH2$Q[2:25]))
SlopeJ_1<-coefficients(RegJ_1)[2]
InterceptJ_1<-coefficients(RegJ_1)[1]
summary(RegJ_1)
residualsJ1<-(resid(RegJ_1))
ccf(resid(RegJ_1),RegJ_1$fitted.values, main="JSP2, LR", ylim=c(-0.6,0.6))

#JSP2, 1 h lag
RegJ_2<-lm(log10(JH2$SSC[25:96])~log10(JH2$Q[26:97]))
SlopeJ_2<-coefficients(RegJ_2)[2]
InterceptJ_2<-coefficients(RegJ_2)[1]
summary(RegJ_2)
residualsJ2<-(resid(RegJ_2))
ccf(resid(RegJ_2),RegJ_2$fitted.values, main="JSP2, LR", ylim=c(-0.6,0.6))

#JSP3, 1 h lag
RegJ_3<-lm(log10(JH2$SSC[96:201])~log10(JH2$Q[97:202]))
SlopeJ_3<-coefficients(RegJ_3)[2]
InterceptJ_3<-coefficients(RegJ_3)[1]
summary(RegJ_3)
residualsJ3<-(resid(RegJ_3))
ccf(resid(RegJ_3),RegJ_3$fitted.values, main="JSP3, LR", ylim=c(-0.6,0.6))

#Merge residuals from individual subperiods
ResidualsJ<-c(residualsJ1, residualsJ2, residualsJ3)
SmoothIndexResidualsSPJ <- rollmean(x = ResidualsJ, # original series
width=24, # width of the rolling window
k=24)

#Plot residuals with 24 h mean in color
d2 = data.frame(x=TimeDateJH2,y=SmoothIndexResidualsSPJ,z=ResidualsJ)
Resid_July2<-ggplot(d2, aes(x,y))
+ geom_area(data=subset(d2, y<=0), fill="darkblue")
+ geom_area(data=subset(d2, y>=0), fill="darkorange")
+ scale_x_chron()
+ scale_y_discrete(limits=c(-1.5,-1,-0.5,0,0.5,1,1.5))
+geom_line(aes(x,z), color="darkgrey")
+ geom_line(aes(x,y))
+ xlab("")+ylab("Residual, SSC") + ggtitle("July")

#Plot residuals July and August
grid.arrange(Resid_July2, Resid_August2)

```

```

#Create lines from generated equations
yJ1=(InterceptJ_1+log10(JH2$Q[2:25])*SlopeJ_1)
yJ2=(InterceptJ_2+log10(JH2$Q[26:97])*SlopeJ_2)
yJ3=(InterceptJ_3+log10(JH2$Q[97:202])*SlopeJ_3)
Ytot=(InterceptJ+log10(JH2$Cross_area)*SlopeJ)

#Plot all subperiods, July and August.
#Data points and fitted lines with 95 % confidence interval.
ggplot(plotJSP, aes(QJ1, SSCJ1))+geom_point(color="yellow")
+ stat_smooth(method="lm", color="yellow")
+ geom_point(data=plotJSP, aes(x=QJ2, y=SSCJ2), color="red")
+ stat_smooth(data=plotJSP, aes(x=QJ2, y=SSCJ2), method="lm",
color="red")
+ geom_point(data=plotJSP, aes(x=QJ3, y=SSCJ3), color="darkred")
+ stat_smooth(data=plotJSP, aes(x=QJ3, y=SSCJ3), method="lm",
color="darkred")
+ geom_point(data=plotJSP, aes(x=QJ4, y=SSCJ4), color="darkorange")
+ stat_smooth(data=plotJSP, aes(x=QJ4, y=SSCJ4), method="lm",
color="darkorange")
+ geom_point(data=plotJSP, aes(x=QA1, y=SSCA1), color="darkblue")
+ stat_smooth(data=plotJSP, aes(x=QA1, y=SSCA1), method="lm",
color="darkblue")
+ geom_point(data=plotJSP, aes(x=QA2, y=SSCA2), color="blue")
+ stat_smooth(data=plotJSP, aes(x=QA2, y=SSCA2), method="lm",
color="blue")
+ geom_point(data=plotJSP, aes(x=QA3, y=SSCA3), color="green")
+ stat_smooth(data=plotJSP, aes(x=QA3, y=SSCA3), method="lm",
color="green")
+ geom_point(data=plotJSP, aes(x=QA4, y=SSCA4), color="black")
+ stat_smooth(data=plotJSP, aes(x=QA4, y=SSCA4), method="lm",
color="black")
+ geom_point(data=plotJSP, aes(x=QA5, y=SSCA5), color="darkgreen")
+ stat_smooth(data=plotJSP, aes(x=QA5, y=SSCA5), method="lm",
color="darkgreen")
+ show.legend = TRUE
+ show_guide(values=c("yellow", "red", "darkred", "darkorange", "darkblue",
"blue", "green", "black", "darkgreen"))
+ labels=c("JSP1", "JSP2", "JSP3", "JSP4", "ASP1", "ASP2", "ASP3", "ASP4", "ASP5"))
+ ylab("SSC_ [g/l]") + xlab("Q_ [m3/s]")
+ scale_y_log10(breaks=c(.1, 1, 10), labels=c(.1, 1, 10))
+ scale_x_log10(breaks=c(.01, .1, .5), labels=c(.01, .1, .5))
+ theme(axis.text.x = element_text(size=12, face="bold"))
+ theme(axis.text.y = element_text(size=12, face="bold"))
+ theme(axis.title=element_text(size=14, face="bold"))

#Plot linear regression all subperiod.
# Fitted lines with 95% confidence interval.
ggplot(plotJSP, aes(QJ1, SSCJ1))
+ stat_smooth(method="lm", color="yellow")

```

```

+ stat_smooth(data=plotJSP , aes (x=QJ2,y=SSCJ2) ,
method = "lm" , color = "red")
+ stat_smooth(data=plotJSP , aes (x=QJ3,y=SSCJ3) ,
method = "lm" , color = "darkred")
+ stat_smooth(data=plotJSP , aes (x=QJ4,y=SSCJ4) ,
method = "lm" , color = "darkorange")
+ stat_smooth(data=plotJSP , aes (x=QA1,y=SSCA1) ,
method = "lm" , color = "darkblue")
+ stat_smooth(data=plotJSP , aes (x=QA2,y=SSCA2) ,
method = "lm" , color = "blue")
+ stat_smooth(data=plotJSP , aes (x=QA32,y=SSCA32) ,
method = "lm" , color = "green")
+ stat_smooth(data=plotJSP , aes (x=QA4,y=SSCA4) ,
method = "lm" , color = "black")
+ stat_smooth(data=plotJSP , aes (x=QA5,y=SSCA5) ,
method = "lm" , color = "darkgreen")+
+ show.legend = TRUE
+show_guide(values=c("yellow" ," red" ," darkred" ," darkorange" ," darkblue" ,
" blue" ," green" ," black" ," darkgreen" )
+ labels=c("JSP1" ," JSP2" ," JSP3" ," JSP4" ," ASP1" ," ASP2" ," ASP3" ," ASP4" ," ASP5" ))
+scale_y_log10(breaks=c(.1,1,10),labels=c(.1,1,10))
+scale_x_log10(breaks=c(.01,.1,.5),labels=c(.01,.1,.5))
+ theme(axis.text.x = element_text(size=12,face="bold"))
+ theme(axis.text.y = element_text(size=12,face="bold"))
+ theme(axis.title=element_text(size=14,face="bold"))

```

APPENDIX E. Moving window regression

R code for moving window regression. Example showing moving window regression performed for July.

```
#Set working directory
setwd("C:/Users/Marie/Desktop/R")
#Load packages
library(chron) #To work with time series considering time and date
library(xts) #Also loads zoo, to use the rollapply function
#Accept NA
na.rm=TRUE

#Load data for hourly values
JH2=read.csv("J_hourly_full_2_10.csv")
#Create a chron object, time serie combining date and time
dtsJH2<-(JH2$Date)
tmsJH2<-(JH2$Time)
TimeDateJH2 <- chron(dates = dtsJH2, times = tmsJH2,
format = c(dates="m/d/y", times="h:m:s"))

#Create an xts object with column 3:12 from JH2.
XJ<-xts(JH2[3:12], order.by=TimeDateJH2)
#Create a zoo object containing turbidity (column 1)
#and Q (column 9). Inputs must be xts objects.
ZJ <- cbind(x = as.zoo(XJ)[, 9], y = as.zoo(XJ)[, 1])

#Save coefficients from log-log linear regression, i.e. slopes and intercepts.
Coef <- function(m) coef(lm(log10(y) ~ log10(x), as.data.frame(m)))

#Perform a running regression,
#starting the next regression 24 h later than the previous.
roll <- function(w) rollapply(ZJ, w, Coef, by = 24, by.column = FALSE)

#Defining the length of the subperiods, 24 - 168 hours.
#For every window adding 24 hours.
widths <- seq(24, 168, 24)

#Perform running regression subperiods of length = widths.
#Name every windows running regression after window size (in hour)
L <- lapply(widths, roll)
names(L) <- widths

#Merge obtained intercepts and slopes into two vectors.
intercepts <- do.call("merge", lapply(L, "[", TRUE, 1)) # extract 1st column
slopes <- do.call("merge", lapply(L, "[", TRUE, 2)) # 2nd columns
#Fill in missing values as NA.
Intercepts <- na.fill(intercepts, list(NA, "extend", NA))
Slopes <- na.fill(slopes, list(NA, "extend", NA))
#Plot intercepts and slopes.
plot(Intercepts)
plot(Slopes)
```

APPENDIX F. Intercepts from moving window regression

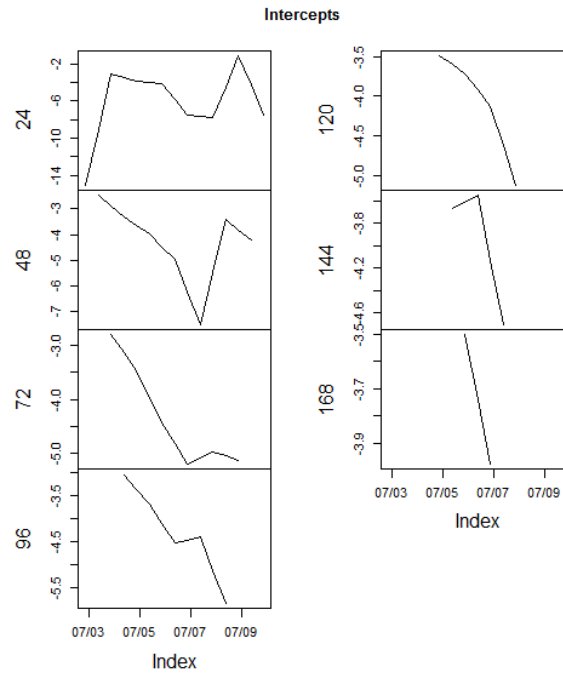


Figure F1: Intercepts from running regression for July. Length of subperiod is indicated in hours on the left side of the panels.

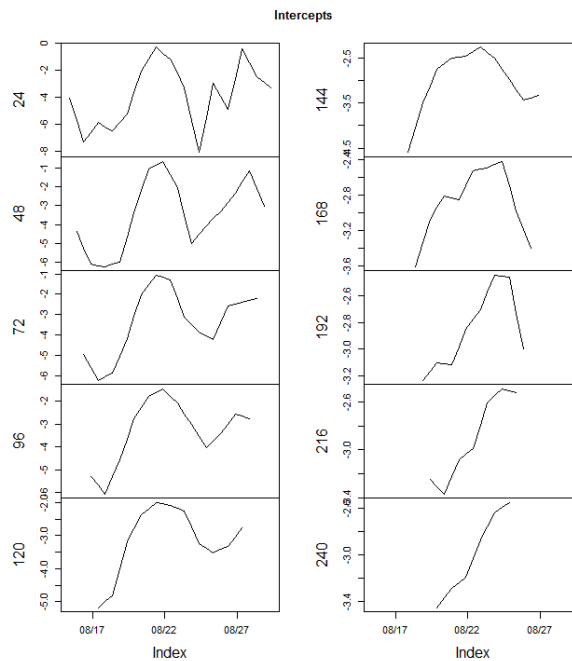


Figure F2: Intercepts from running regression for August. Length of subperiod is indicated in hours on the left side of the panels.

APPENDIX G. Multiple linear regression

R code used for multiple regression, example showing code for JSP1.

```
#Set working directory
setwd("C:/Users/Marie/Desktop/R")
#Load packages
library(chron) #To work with time series considering time and date
#Except NA
na.rm=TRUE
options(stringsAsFactors=FALSE)

#Load data with hourly values for JIuy
JH2=read.csv("J_hourly_full_2_10.csv")

#create a chron object, time serie combining date and time
dtsJH2<-(JH2$Date)
tmsJH2<-(JH2$Time)
TimeDateJH2 <- chron(dates = dtsJH2, times = tmsJH2,
format = c(dates="m/d/y", times="h:m:s"))

#First explanatory variables were prepared.

#Calculate hours since discharge was equaled or exceeded for July.
#That is the amount of hours since the discharge was
#equal to or bigger than previous discharge.

#Create vector of same length as data set.
Hours_EE_J <- numeric(length(JH2$Q))

#Find hours since Q was equal or exceeded.
for (i in 1 : length(JH2$Q)) {
  less_or_eq <- JH2$Q[1 : i] <= JH2$Q[i]
  if (all(less_or_eq)) {
    Hours_EE_J[i] <- 0
  } else {
    inds <- which(less_or_eq == 0)
    Hours_EE_J[i] <- (i - inds[length(inds)])
  }
}

#Show result.
Hours_EE_J
#Save results as csv
write.csv(Hours_EE_J, file="hours_EE")

#Example of multiple regression analysis performed
#for the first subperiod of July.
#During the first regression, all variables were included.
#The less significant were then excluded by adding #
```

```

J_MR1<-lm(log(JH2$Turbidity[1:24])~
          log(JH2$Cross_area[2:25])+
          JH2$DLOGQ2[1:24]
          #+JH2$Hour_EE[1:24]
          #JH2$h_sp_beg[1:24]
          #+JH2$P1[1:24]
          #+JH2$P2[1:24]
          #+JH2$P3[1:24]
          #+JH2$P4[1:24]
          #+JH2$P6[1:24]
          #+JH2$P1_1[1:24]
          #+JH2$P2_1[1:24]
          #+JH2$P3_1[1:24]
          #+JH2$P4_1[1:24]
          #+JH2$P6_1[1:24]
          #+JH2$P1_2[1:24]
          #+JH2$P2_2[1:24]
          #+JH2$P3_2[1:24]
          #+JH2$P4_2[1:24]
          #+JH2$P6_2[1:24]
          #+JH2$P1_3[1:24]
          #+JH2$P2_3[1:24]
          #+JH2$P3_3[1:24]
          #+JH2$P4_3[1:24]
          #+JH2$P6_3[1:24]
          )

#Show summary of the statistics.
summary(J_MR1)
#Plot autocorrelation function.
ccf(resid(J_MR1),J_MR1$fitted.values, main="JSP1, _MR", ylim=c(-0.6,0.6))

```